Chapter 1

Measurement of absolute cross sections of electron scattering by isolated molecules

Michael Allan

Department of Chemistry, University of Fribourg, CH-1700 Fribourg, Switzerland

1.1 Introduction

There is twofold interest in the measurement of the various quantitative cross sections described in this chapter. The first is direct use of the measured quantities to understand and to model systems where electron-molecule (atom) collisions occur, that is, technological plasmas, upper partially ionized layers of planetary atmospheres, comets, but also in flames. The second is providing data for testing various theories. The two areas are related. Experiments can not measure all the quantities required for the applications, it is very hard to measure for example cross sections for reactive intermediates and for electronically excited atoms and molecules and these quantities must be provided by theory. On the other hand development of theory is not possible without experimental data for comparison.

The electron scattering research is not new, pioneering studies date from the 1930's and has been revived by the discovery of resonances in late 1960's (Schulz 1973). But the field goes through a phase of intense activity, caused by novel areas of application (radiation therapy, nanofabrication), improvement of instrumentation permitting observation not available in the past, and by improvement of theory and computational power leading to demand for new experimental data for comparison.

Recently, there has been increasing emphasis on the processes which cause chemical change and thus promise to be useful in plasma chemistry, material science or radiation therapy. They include the dissociative electron attachment (DEA), electronic excitation followed by dissociation, and dissociative ionization.

The measurements of DEA and vibrational excitation (VE), on which this chapter concentrates, are complementary, and ideally both should be measured for each compound. This is because the important electron-driven processes proceed *via* resonances (temporary negative ions) and the various processes described here are often competing decay channels of the same resonances and thus a combined knowledge provides more detailed information on them. In particular, bands in VE cross sections provide valuable information on resonances, helpful for understanding DEA.

Resonant electron induced processes start with a vertical attachment of an electron to a molecule – the anion has initially the geometry of the target. The anion then starts to relax, it distorts as a consequence of modifications of bonding caused by the extra electron. The distortion may be trivial, for example the C≡C or C=C bond lengthens because the π^* orbital into which the extra electron is accommodated is antibonding along the bond, or less trivial, like the symmetry lowering (Renner-Teller effect) related to vibronic coupling (Estrada et al. 1986). In the process of this relaxation, autodetachment proceeds at a rate given by the width Γ of the resonance at each particular geometry, leading generally to a vibrationally excited state of the neutral molecule. The selectivity into which vibrational mode the resonance decays, and how many quanta are excited, are indicative of what geometry change occurred in the process of the relaxation, as outlined in the pioneering study of Walker et al. 1978. DEA is competing with the VE; it is due to those anions which survived, did not autodetach, and whose geometry has distorted beyond the stabilization point – the crossing of the anion and neutral potential surfaces. The information about the path of the relaxation, derived from the VE, can thus help in understanding DEA.

This chapter starts by presenting some of the experimental technique used to measure various absolute cross sections, focusing on the instrumentation used in Fribourg. It will then present a selection of examples, highlighting some of the interesting areas, such as shape and core excited resonances and the use of vibrational excitation, in particular the selectivity of vibrational excitation, to obtain detailed information on the resonances, threshold phenomena, in particular vibrational Feshbach resonances (VFR), and the selectivity and the mechanisms of dissociative electron attachment.

1.2 Experimental methods

1.2.1 Electron scattering

The basic quantity of electron scattering is the grand total cross section σ_T which can be derived from the attenuation of an electron beam traversing a chamber of a given length and with a known sample pressure in a transmission experiment. Pioneering studies were performed by Ramsauer and Kollath who reached surprisingly low energies and whose results were proven correct by later experiments. They applied their method to rare gases (Ramsauer and Kollath 1929), where they discovered the Ramsauer-Townsend minimum, and to small molecules (Ramsauer and Kollath 1930). The more modern version of this instrument uses an axial magnetic field and the publications of the Gdańsk group are representative for this type of work (see, for example Szmytkowski et al. 1996). The principle problem of this method is the incomplete discrimination agains electron scattered into nearly forward direction. Apart from this, the data is very reliable because of the

simplicity of the experiment and are valuable as a verification of the partial and differential cross sections. The integration of differential cross sections over all angles to yield the integral partial cross section, and their sum for all accessible processes yields the grand total cross section – and this must agree with the result of the transmission experiment. This important validation of the differential cross section sets will be exemplified on CO below.

The transmission method has been dramatically improved with the development of the "Surko" trap system for positron scattering (Murphy and Surko 1992, Gilbert et al. 1997, Sullivan et al. 2008) and has become remarkably powerful, both because cross sections can be measured with few incident particles, and because partial cross sections (elastic, vibrationally inelastic) can be measured using a retarding field analyzer. Resolution has been greatly improved by cooling the incident electrons in a trap with a buffer gas cooled by liquid nitrogen. The method is equally applicable to measurement of electron collision cross section, and could gain more popularity for this application in the future since it is potentially simpler than the double hemispherical system described below, and has the advantage of measuring integral cross sections which are often sufficient for the application in plasma simulation, by-passing the step of first measuring many differential cross sections and having to integrate them.

The magnetically-collimated electron spectrometer (Allan 1982) using "trochoidal" electron energy analyzers (Stamatovic and Schulz 1968) can in some cases also be used to measure absolute inelastic cross sections, when an assumption about the angular distributions can be made and when suitable absolute data for normalization is available; an example is the work on H_2 (Poparić et al. 2010). This instrument has certain advantages – very high sensitivity and low energy capacity, and the capacity to measure the $0°/180°$ cross section ratio.

The standard instrument to measure differential cross sections is a spectrometer with electrostatic analyzers. Although the principle is not new (see for example Pavlovic et al. 1972) it has been substantially improved over the past years, in terms of low-energy capacity, extanding the angular capacity to the full angular range $0° - 180°$, improving the correction for the instrumental response function, and the resolution. This chapter will concentrate on this type of instrument, in particular the version developed in Fribourg.

Double hemispherical instrument

The Fribourg spectrometer with hemispherical analyzers has been constructed already in the late 1980's, but has been continuously improved (Allan 1992, Allan 2005, Allan 2007a, Allan 2010). The energy resolution is typically about 15 meV in the energy-loss mode, corresponding to about 10 meV in the incident electron beam, at a beam current of around 400 pA, although a beam current of 2 nA can be reached at a resolution of 25 meV, and a resolution of 7 meV was reached with a current of 40 pA (Allan 2001). The energy of the incident beam is calibrated on the 19.365 eV (Gopalan et al. 2003) ^{2}S resonance in helium and is accurate to within ± 10 meV. The instrumental response function was determined on elastic scattering in helium and all spectra were corrected as described earlier (Allan 2005).

Absolute values of the elastic cross sections are determined by the relative flow technique as described by Nickel et al. 1989 using the theoretical helium elastic cross sections

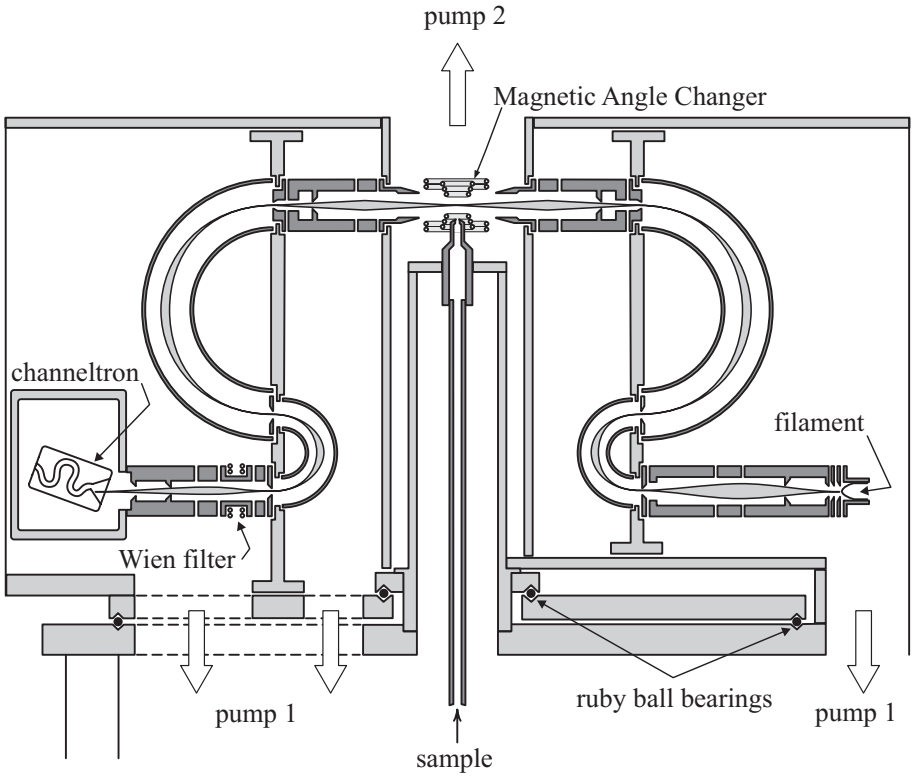

Figure 1.1: Schematic diagram of the Fribourg double hemispherical spectrometer (Allan 2004). Reprinted with permission from M. Allan, Threshold phenomena in electron-molecule scattering. Phys. Scripta 2004, **T110**, 161-165. Copyright 2004 IOP Publishing Ltd.

of Nesbet 1979 as a reference. The confidence limit is about ±20% for the elastic cross sections and ±25% for the inelastic cross sections (two standard deviations). The sample and helium pressures in the gas inlet line during the absolute measurements were kept low, typically 0.1 and 0.2 mbars, respectively. Background is determined by recording signal with gas flowing into the main chamber *via* a by-pass line and not the nozzle. This background is generally negligible except in the more forward scattering and at low energies. The excitation functions and the angular distributions are measured at higher pressures and background is subtracted only when it is significant. Absolute inelastic cross sections are derived by integrating the areas under the elastic and inelastic peaks in energy-loss spectra recorded at constant incident energies, corrected for instrumental response functions, and normalizing to the elastic cross section measured by the relative flow method.

The instrument incorporates the magnetic angle changer (MAC) invented by Read and coworkers (Read and Channing 1996, Zubek et al. 1996), which permits measurements of scattering into the backward hemisphere. The particular form of the MAC realized in Fribourg (Allan 2000, Allan 2004) is made of few windings of a thin (0.63 mm diameter) copper tubing, cooled by water. This design minimizes the obstruction of the gas flow,

the local pumping speed in the collision region is nearly unaffected by the presence of the MAC. This reduces beam attenuation by background gas, is important for absolute measurements which rely on a definite gas flow, and improves resolution by reducing thermal Doppler broadening encountered in scattering by the background gas. The design further simplifies the power supplies since it has only one current loop for both the inner and the outer solenoids. The same computer controls the digital-to-analog convertors determining the incident and the scattered electron energies (E_i and E_r) and the MAC current, which is automatically adjusted to provide the desired deflection angle every time E_i and/or E_r are changed. The scattering angle was calibrated by guiding the incident beam into a rotatable Faraday cup and is accurate within $\pm 3°$.

The angular distributions are measured using combined mechanical setting of the analyzer and magnetic deflection with the magnetic angle changer (Read and Channing 1996, Zubek et al. 1996, Zubek et al. 2000, Cho et al. 2004), correcting the curves for the instrumental response function (determined on helium and, for angles near 0°, on the $v = 1$ excitation cross section in N_2), and fitting them to the discrete absolute values measured at 45°, 90°, 135° and 180°. Details of the procedure were described by Allan 2005. The magnetic deflection is typically incremented in steps of 1 or 2.5°.

Peak widths often depend on energy and scattering angle. One reason is the Doppler broadening which makes peaks of light targets wider at large scattering angles and higher energies. Another frequent reason is rotational excitation which is, particularly in a resonance region, strong (see Jung et al. 1982 for examples), and leads to a substantial broadening of the energy-loss bands. Consequently, care has to be taken to derive all cross sections from the areas under the energy-loss bands and not from their heights. For angular distributions, and for the absolute measurements, an energy-loss peak is recorded at each energy and angle, which is then numerically integrated. Two methods are used for the excitation functions. One consists of recording a number of excitation functions at energy-losses around the nominal energy loss of the process being recorded (elastic or a given vibrational level), thus covering the entire width of rotational excitations, and then making the sum. The other consists of recording a number of energy-loss spectra in the energy range of interest, then deriving numerically their heights and areas and constructing a 'height-to-area correction function', used to correct an excitation function recorded at the top of the energy-loss peak. Both methods gave consistent results.

1.2.2 Dissociative electron attachment

Total ion collection instruments

The importance of knowing absolute cross section for dissociative electron attachment has been realized early. To measure them, an early generation of total ion current collection tubes has been developed, for example by Rapp and Briglia 1965, Azria et al. 1974. The importance of absolute DEA cross sections motivated the group in Lincoln (Aflatooni et al. 2006) and in Fribourg (Fedor et al. 2008) to construct modernized versions of this instrument. A slightly simplified version was constructed in Bologna (Modelli 2005). The principal weakness of this instrument is the background of scattered electrons which, at finite pressure, diffuses across the axial magnetic field which is confining them. This background limits the applications to relatively large cross sections. The great advantage of this method is that it is fundamentally an absolute measurement, it does not rely on normalization to

other data.

Classical mass spectrometer

Early DEA spectra were measured at low resolution with modified commercial mass spectrometers (Dorman 1966). These instruments were very sensitive, but did not yield absolute DEA cross section values. The workhorse of the majority of research groups studying DEA are quadrupole mass spectrometers. The resolution of the electron beam is generally improved by using a trochoidal electron monochromator (Stamatovic and Schulz 1968), sometimes electrostatic analysers (Vizcaino et al. 2010). These instruments yielded a wealth of most interesting information, recently particularly related to biologically relevant molecules (Ptasinska et al. 2005). The majority of these instruments does not, however, measure the absolute cross sections.

Velocity imaging spectrometers

An exciting new development in the instrumentation for dissociative electron attachment are the velocity imaging techniques. They are based on the COLTRIMS technique developed originally for photodissociation experiments and employ a pulsed electron beam to prevent its perturbation by the ion extraction field and to permit time-of-flight (TOF) analysis of the ions. Two versions of this instrument are currently in operation, the velocity slice technique in Mumbai (Nandi et al. 2011) and the COLTRIMS technique in Berkeley (Adaniya et al. 2009).

Quantitative time-of-flight spectrometer

This section describes the instrument constructed in Fribourg, combining TOF with the total ion collection technique. More detailed descriptions were given by Fedor et al. 2008 and May et al. 2009. An alternative scheme, a TOF spectrometer measuring absolute DEA cross section by the relative flow technique, is operated in Mumbai (Prabhudesaia et al. 2005).

Schematic diagram of the instrument is shown in Fig. 1.2. The instrument uses axial magnetic field to collimate the electrons and a trochoidal electron monochromator to reduce the electron energy spread. The collision chamber is equipped with an exit slit through which ions enter a time-of-flight (TOF) tube. A short (200 ns) pulse of electrons is sent through the interaction region while the ion repellers are on the potential of the chamber. A 4μs long pulse with an amplitude between -300 and -450 V is applied to the repellers about 200 ns later, after the electrons have left the collision chamber. The experiment is repeated at a rate of between 10 and 100 kHz.

Measurements of absolute cross sections require that the spectrometer is 'quantitative', i.e., that the ion collection efficiency does not depend on their mass and their initial kinetic energy. The dependence on mass is given primarily by the fact that the ions have to traverse magnetic field required for collimation of the electron beam. The curving of their trajectories is compensated by electrostatic deflectors in the first stage of the ion drift tube. The latter criterion is fulfilled by using a relatively high repeller voltage, accelerating the ions to energies much higher than their initial kinetic energy, and by using a slit 10 mm wide in the direction perpendicular to the direction of the electron beam. The yield of

ions is further controlled by the focusing voltage on the center element of the ion drift tube, functioning as a zoom lens.

Another potential problem stems from the fact that ions formed in the early stages of the electron beam pulse have time to travel a certain distance before the repeller pulse arrives, reducing their chance of being collected. This problem can be reduced, at the expense of signal intensity, by reducing the electron beam pulse duration. Ion trajectory calculations indicate that the design has a constant collection efficiency up to an initial ion kinetic energy of 2.5 eV, and retains 90% of it up to about 4 eV.

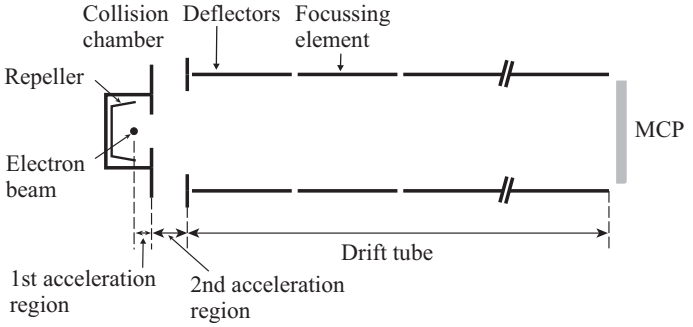

Figure 1.2: Schematic diagram of the Fribourg TOF spectrometer for absolute DEA cross sections (May et al. 2009). The orientation of electron beam is perpendicular to the paper plane. Reprinted with permission from O. May, J. Fedor, M. Allan, Isotope effect in dissociative electron attachment to acetylene. Phys. Rev. A 2009 **80**, 012706. Copyright 2009 American Physical Society.

The ions which passed the TOF tube are detected with a microchannel plate (MCP), counted, and their arrival times are analyzed using the delayed coincidence scheme, with a time-to-amplitude converter (TAC) and a pulse-height analysis.

An additional potential problem with respect to the requirement of a 'quantitative' mass spectrometer stems from the possible dependence of the detector efficiency on the type of ion. This problem is by-passed by accelerating the ions to very high energies, where the quantum yields for all ions concerned saturate. We have found that the quantum yield of the detector saturates already at 3 kV for all ions investigated (O^-, C_2H^-, C_2^-, H^-).

The pressure in the collision chamber is measured by a capacitance manometer and is kept typically between 0.3×10^{-3} and 0.6×10^{-3} Torr during the measurement. The cross sections were normalized on the 4.4 eV, O^-/CO_2 DEA band. The measurements of this cross section have been reviewed by Orient and Srivastava 1983 and by Itikawa 2002. We take a value of 14 pm^2, which is the average of the values listed by Orient and Srivastava, together with our own value from the total ion collection experiment. The entire TOF scheme was verified by measuring the cross sections for the O^-/N_2O and O^-/O_2 processes, with the correct results.

The thermionic cathode warms the target chamber to about 60°C (measured by a Pt100 probe) during operation, making the Knudsen correction (Knudsen 1910) necessary in the total ion collection mode. This correction is redundant in the case of time-of-flight measurements because it applies in the same way to both the measured gas and the calibrating gas CO_2.

1.2.3 Neutral dissociation

Neutral dissociation, fragmentation which leads only to neutral fragments, is an important process in plasmas and other applications. It has been neglected experimentally because of the difficulty to detect neutral fragments, as opposed to charged fragments, which can be detected with high sensitivity using mass filters and electron multipliers. A more comprehensive account of the techniques, results, and associated problems have been described in a recent review (Moore et al. 2010).

There were few efforts to detect the neutral fragments by ionizing them by electron impact and then using a quadrupole mass spectrometer. The method suffers from the fact that the concentration of radicals to be ionized and detected is typically orders of magnitude less than that of the parent gas and that electron-impact ionization of the radicals yields the same masses as dissociative ionization of the parent. The electron ionizer of the mass spectrometer must therefore operate with low electron energies, just above the ionization energy (IE) of the radical to be detected, but below the IE of the parent. This results in low sensitivity because ionization efficiency is low near threshold. This scheme has been realized by Sugai and collaborators (Tanaka et al. 1998).

A more powerful and nearly universal technique for the quantitative analysis of radicals has been developed by Motlagh and Moore 1998 at the University of Maryland. The technique, based on the method by which radicals in the gas phase were first identified, relies upon the efficient reaction of radicals with tellurium to yield volatile and stable organotellurides. A beam of electrons passes through a target gas in a collision cell that has a tellurium mirror on its inner surface. Radicals from electron-impact fragmentation react with tellurium within their first few encounters with the wall to produce volatile tellurides. The telluride partial pressure is measured mass spectrometrically and related to the radical production rate. The technique is specific for radicals since a target gas of stable (closed-shell) molecules does not react at the tellurium surface. In addition, the portion of the mass spectrum under observation is displaced by more than 128 amu (the nominal tellurium mass) from the region displaying peaks characteristic of the parent gas – by-passing the problem of having the same masses as fragments of the parent molecule.

This method has been employed to measure *partial* cross sections for the production of neutrals by electron impact on CH_4, CH_3F, CH_2F_2, CHF_3, CF_4, C_2F_6 and C_3F_8 (Motlagh and Moore 1998). The instrument is, however, no longer operational and there is worldwide no laboratory having this important technique.

1.3 Nitrogen

N_2 is perhaps the most studied molecule as far as electron collisions are concerned, both experimentally and theoretically, and is suitable for verifying new methods, both experimental and theoretical. It will therefore be taken as the example on which the experimental procedures will be explained. This chapter reviews the work of the article of Allan 2005, which also lists references to earlier work. Particular mention deserves the paper by Zubek et al. 2000 who used the MAC to extend the elastic and the $v = 0 \rightarrow 1$ differential measurements to 180°.

1.3.1 Procedures of measuring absolute cross sections

Tuning

It is essential to obtain an optimal beam focus, and an optimal overlap of the three entities incident beam, analyzer acceptance cone (the 'scattered beam'), and the gas beam, when the electron energies E_i and E_r and the scattering angle θ are changed. The 6 voltages which control these parameters, that is the two voltages on the central cylinders of the zoom lenses at the monochromator exit and the analyzer entrance, and the x and y deflector voltages of these two lenses, are empirically optimized for maximum signal at a number of energies and angles (the 'pivotal points'), the values are stored, and the instrument then automatically sets the values interpolated between the pivotal points. This procedure is called 'tuning' and a 'tuned' instrument can be used as a 'black box', that is, the incident and residual energies and the scattering angle, may be scanned and the optimal overlap is maintained automatically. The performance needs to be frequently verified on He, and the instrument re-tuned, to offset surface potential drifts.

There is a subtle point in this procedure: not only must the incident and scattered beams overlap optimally for all energies and angles, but the distance of the overlap point from the gas nozzle must remain constant as E_i and E_r are changed. If this is not the case, then the instrument yields optimum signal for elastic scattering, but the signal for inelastic scattering can be reduced dramaticaly. This desired condition is reached by adjusting the analyzer x and y deflector voltages for low energies ($E_r = 0 - 5$ eV) on deeply inelastic scattering (2^3S and 2^3P excitation) from He. While doing so the incident beam's energy is in the range of 20-25 eV, that is, it is high and changes only by a relatively small percentage – the distance of the incident beam from the nozzle is nearly constant within this range of the incident energies. The analyzer tuned to the incident beam in this way has consequently also a nearly constant distance from the nozzle even when E_r is changed. The monochromator is then tuned in the $E_i = 0 - 5$ eV range on elastic scattering, that is, to the scattered beam position, which has been assured to be fixed in the previous step. Elastic signal cannot be measured below $\theta = 10°$ and inelastic signal (for example $v = 0 \rightarrow 1$ in N_2) must be used for tuning at 0°.

Response function for energy scans

The response function for elastic signal is relatively easy to determine, by measuring the He elastic signal as a function of energy and dividing it point by point by the theoretical cross section given by Nesbet 1979. In practice a problem arises because thermal Doppler broadening and shift of the elastic peak due to momentum transfer are not negligible in He as analysed in detail by Read 1975 (see Fig. 1.3). The translational excitation is about 9 meV at 20 eV and 135°. The thermal Doppler broadening increases with θ and with the electron energy, but it also depends on θ for apparative reasons. It is smallest at 90° where the incident and scattered electron beams intersect in a very small volume, (approximately a sphere of about 0.25 mm diameter) in the present instrument, in the front of the nozzle, and the molecules in this effective collision volume move all essentially in one direction. The apparative aspect is worst near 0° and 180° where the incident and scattered electron beams are nearly collinear, probe the effusive gas beam over a large length, with a substantial range of directions of the thermal velocities of the target gas.

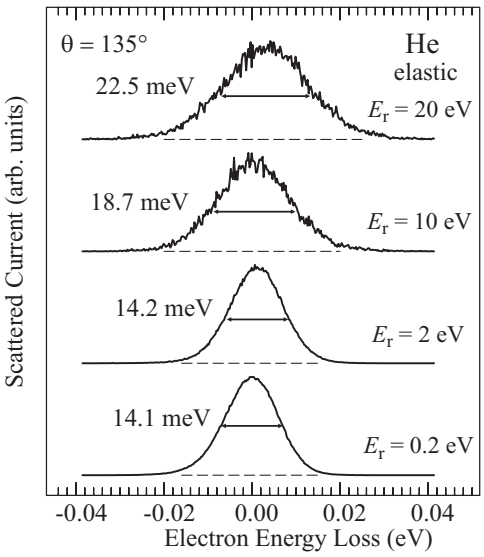

Figure 1.3: Energy-loss profiles of the He elastic line, illustrating the Doppler-broadening at higher energies.

As a consequence the elastic peak becomes broader and shifts to higher energy loss ΔE with increasing scattering angle and increasing incident electron energy E_i. The width of the He elastic peak was 14 meV at 0.4 eV and 22.5 meV at 20 eV at $\theta = 135°$ (Fig. 1.3) during the N_2 measurements, indicating a Doppler broadening of 17.6 meV. This is still substantially less than the 45 meV calculated for a stationary sample gas using the expression given by Read 1975. The Doppler broadening is particularly pronounced around 180° where the apparative and inherent effects combine and the width of the elastic peak in helium may reach 50 meV. The consequence is that the area under the elastic or inelastic energy-loss peak must be taken in all measurements, not the peak height. In practice this can be achieved either by recording the peak signal and correcting it by a smooth function expressing the area/height ratio measured at a few discrete energies, or by measuring many excitation functions at energy losses spanning the range of about (-50 meV; +50 meV), that is, covering the entire elastic peak, and then taking the sum. The latter method was used in the illustrative example shown in Fig. 1.4.

In theory, the ideal response function should behave as $1/E_r$, because the ideal incident beam is constant and the analyzer acceptance angle should increase with decreasing E_r. The hemispheres operate at a constant pass energy ($1.4-5$ eV for this instrument, 3 eV for the N_2 measurements in this chapter), that is, the pencil angle, defined by the size of the pupil apertures, is constant between the hemispheres. The analyzer entrance pencil angle then increases as $1/\sqrt{E_r}$, the solid entrance angle as $1/E_r$, with decreasing E_r. This is true provided that the magnification of the analyzer entrance lens does not vary significantly with energy. Trajectory calculations (using the program of Read and Bowring 2005) indicate that this assumption is approximately true. At low energies the pencil angle given by this relation exceeds the useful physical dimension of the entrance lens (*i.e.*, the filling factor exceeds 50%), and the acceptance angle cannot grow any further. The response

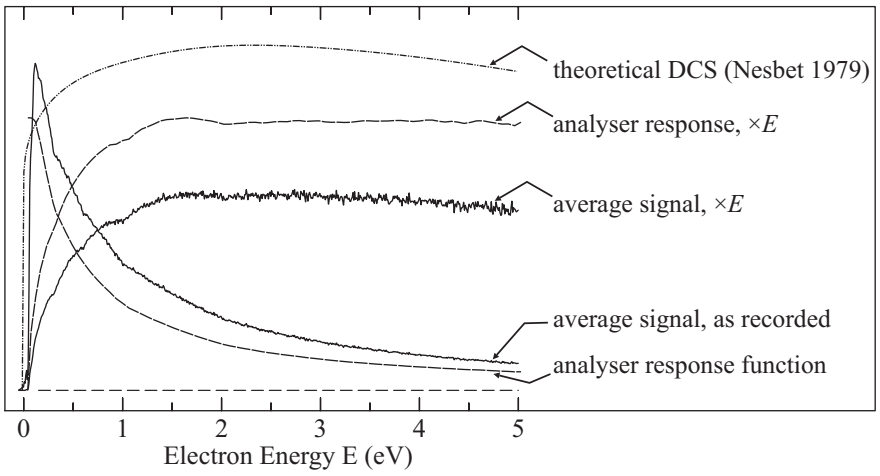

Figure 1.4: Figure illustrating how the variation of response function with electron energy is derived. Some of the curves are shown multiplied by the electron energy E to improve the visibility of the deviation from the 'ideal' $1/E$ behavior. The scattering angle is $\theta = 135°$. The vertical scale is linear and shows the signal intensity, response function, and differential He cross section in arbitrary units. Reprinted with permission from M. Allan, Measurement of the elastic and $v = 0-1$ differential electron-N_2 cross sections over a wide angular range. J. Phys. B: At. Mol. Opt. Phys. 2005 **38**, 3655-3672. Copyright 2005 IOP Publishing Ltd.

then increases slower than $1/E_r$ with decreasing energy, and becomes constant at very low energies. At extremely low energies the electrons are lost because of stray fields. The incident electron beam current is constant down to low energies, but the pencil angle increases with decreasing energy until it reaches the useful diameter of the monochromator exit lens. Below this energy the beam starts to decrease. At low energies the incident beam may also lose efficiency because it becomes diffuse or distorted by stray fields.

Figure 1.4 illustrates how the response function is derived. The signal generally drops rapidly with increasing energy and some of the curves are shown multiplied by E_r to facilitate visual judgment of the deviation from the ideal $1/E_r$ behavior. The signal integrated over all ΔE in the range (-50 meV; +50 meV) to by-pass the effect of Doppler broadening is shown both as recorded and multiplied by E_r. The integrated signal divided by the theoretical DCS yields the response function. The curve representing the response function, multiplied by E_r, reveals that the sensitivity of the instrument behaves approximately ideally (as $1/E_r$) at energies $E_r > 1$ eV. At $E_r < 1$ eV the sensitivity still rises with decreasing E_r, but less rapidly than $1/E_r$, following the expectation outlined above. Finally, at $E_r < 100$ meV, the sensitivity drops rapidly, both because the pencil angle of the incident beam exceeds the useful diameter of the monochromator exit lens and because of stray fields. At an energy range of about 50-100 meV this drop may still be taken into account for correcting elastic cross sections by making a response function which follows this drop, but the result is less reliable.

The flat He ionization continuum has been used to derive the response function by a number of groups (Pichou et al. 1978, Brunger et al. 1989, Allan 1992). This method

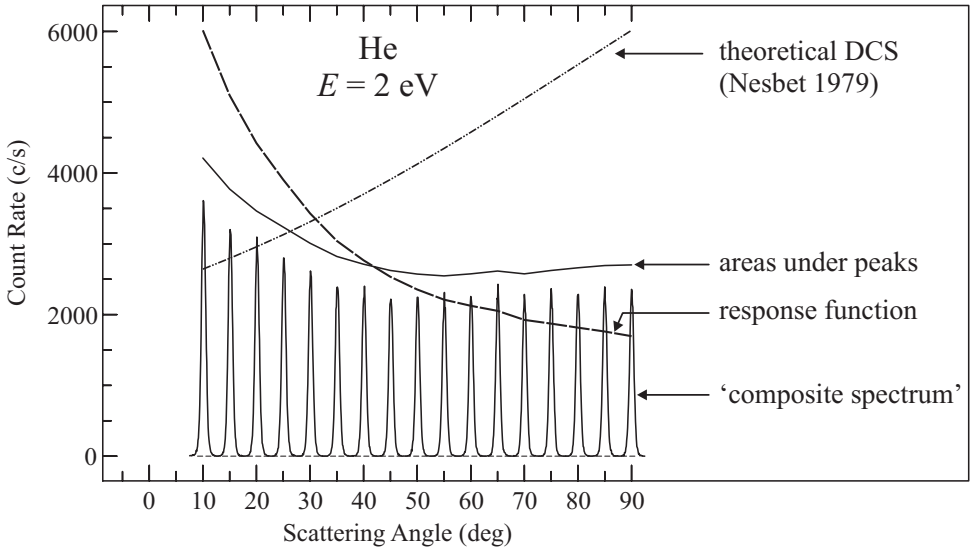

Figure 1.5: Illustration of how the angular response function is generated. Reprinted with permission from M. Allan, Measurement of the elastic and $v = 0 - 1$ differential electron-N_2 cross sections over a wide angular range. J. Phys. B: At. Mol. Opt. Phys. 2005 **38**, 3655-3672. Copyright 2005 IOP Publishing Ltd.

is, however, not suitable for routine response function determination, both because the continuum is flat only for θ not far from 90° (Pichou et al. 1978, Asmis and Allan 1997a) and because the continuum is weak and long accumulation is required during which the instrument drifts.

Response function for angular scans

Experience shows that the present instrument cannot be optimized over the entire angular range with a single set of tuning voltages because of drifts. This problem is circumvented by repetitive magnetical scanning ±45° around one of the three mechanical analyzer positions $\theta = 45°$, 90° and 135°. The steps involved in determining the response function's dependence on scattering angle are illustrated in figure 1.5. A series of short energy-loss spectra around the elastic peak, one at each angle, is recorded. The series is labeled 'composite spectrum' in figure 1.5. The areas under the elastic peaks are then taken and divided by the theoretical DCS to yield the response function. The instrument can not distinguish between nearly forward scattered and unscattered electrons, resulting in a large background for elastic spectra at low angle. The lowest attainable angle is about 15° at 1 eV and slightly below 10° at higher energies.

The resulting response function has a minimum at 90° and increases below and above as the spatial overlap of the incident and scattered beams increases. It levels off near 0° and 180° because the overlap with the target gas beam becomes limiting. For a well tuned instrument the angular response function depends only weakly on energy.

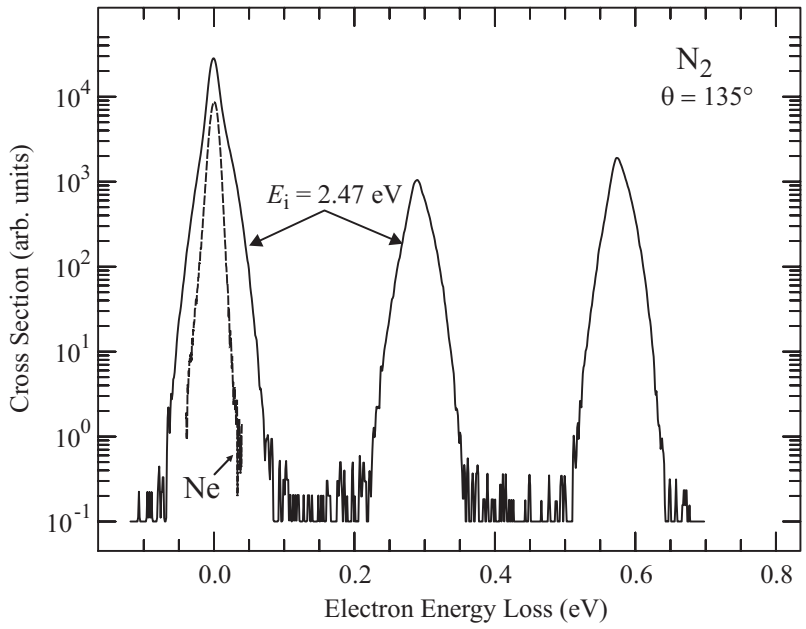

Figure 1.6: Electron energy-loss spectrum used to determine the absolute inelastic cross sections. The elastic peak recorded with neon, representative of the apparatus profile, is also shown. Reprinted with permission from M. Allan, Measurement of the elastic and $v = 0 - 1$ differential electron-N_2 cross sections over a wide angular range. J. Phys. B: At. Mol. Opt. Phys. 2005 **38**, 3655-3672. Copyright 2005 IOP Publishing Ltd.

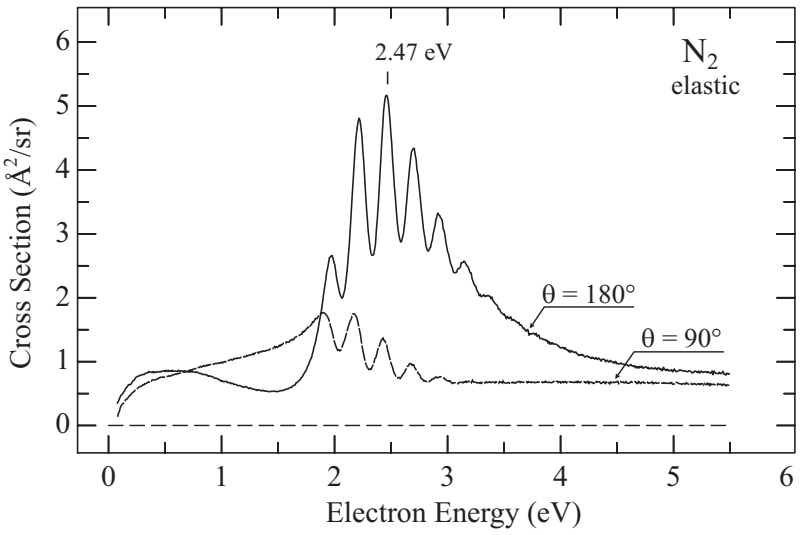

Figure 1.7: Rotationally summed elastic cross sections at 90° and 180°. Data from Allan 2005.

Normalization to absolute values

Absolute elastic cross sections were determined at a number of discrete energies and angles by comparison with the theoretical helium elastic cross section of Nesbet 1979, using the relative flow method, described in detail by Nickel et al. 1989. They are accurate within about ±15%. The energy and angular scans of the elastic signal, corrected for the response functions, are then normalized to the discrete values, with a high degree of redundancy, that is, more discrete values are measured than required, providing a test of consistency of the shapes of the excitation functions.

Absolute inelastic cross sections are obtained by recording energy-loss spectra with constant incident energies at which the elastic cross section has been measured, correcting them for the instrumental response function and deriving the inelastic cross sections from the ratios of areas under the peaks. An example of an energy-loss spectrum is shown in figure 1.6 – it is useful that the background is low, about 5 orders of magnitude below the elastic peak.

1.3.2 Representative results

Energy scans

The two representative energy scans of the elastic cross section shown in Fig. 1.7 illustrate how the shape of the resonant contribution varies with angle as a consequence of the interference with the background scattering. As pointed out by Shi et al. 1993 and Sun et al. 1995, this leads to variations of the positions of the resonant peaks with scattering angle and complicates the comparison of angular distributions obtained by various experiments and by theory. The peak positions found here agree well with those of Sun et al. 1995. The peaks are wide and have a relatively flat top, making determination

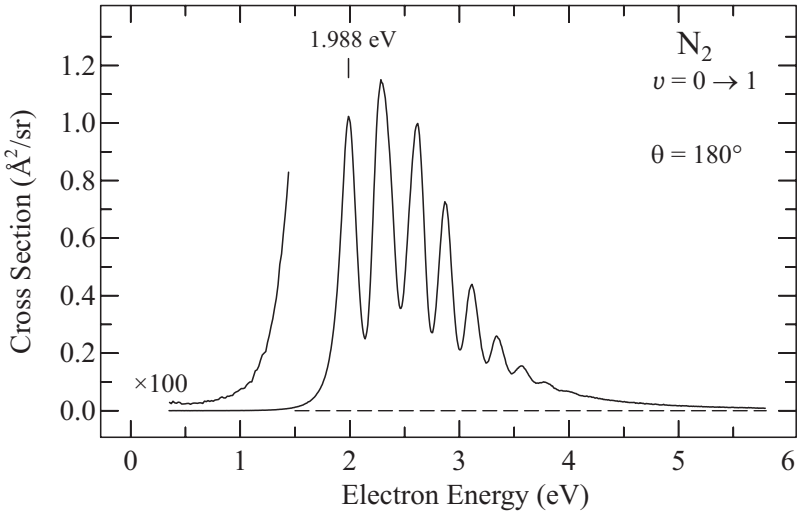

Figure 1.8: The rotationally summed $v = 0 \rightarrow 1$ cross section at 180°. Reprinted with permission from M. Allan, Measurement of the elastic and $v = 0 - 1$ differential electron-N_2 cross sections over a wide angular range. J. Phys. B: At. Mol. Opt. Phys. 2005 **38**, 3655-3672. Copyright 2005 IOP Publishing Ltd.

of the peak position better than about ±15 meV difficult even with precise energy scale calibration. A representative energy scan of the cross section for $v = 1$ excitation is shown in Fig. 1.8

Angular scans

The results for $v = 1$ excitation at the first boomerang peak of the $^2\Pi_g$ resonance are shown in Figure 1.9 as a function of θ. The data is in excellent agreement with the earlier experimental work of Sun et al. 1995 and with the theoretical results of Morrison and coworkers (Feng et al. 2003, Feng et al. 2005). They use the body-frame vibrational close-coupling theory described by Sun et al. 1995.

1.4 Carbon monoxide

This section is based on the recent study of Allan 2010, which was motivated by the data need for simulations of the upper atmospheres of Venus and Mars and cometary comae (Campbell and Brunger 2009a, Campbell and Brunger 2009b, Campbell and Brunger 2008). Electron collisions with CO have been studied many times and references to earlier work were given by Allan 2010. This section concentrates on the methods to obtain integral cross sections from the differential cross sections. An important test of the reliability of the relative flow method to measure absolute cross section is obtained by comparing the grand total cross section obtained from the present partial differential cross sections with the grand total cross section measured directly by the transmission method.

Whereas the elastic cross sections of Allan 2010 are in excellent agreement with those of Gibson et al. 1996, the $v = 1$ cross sections, shown in Fig. 1.10, are about 20% higher

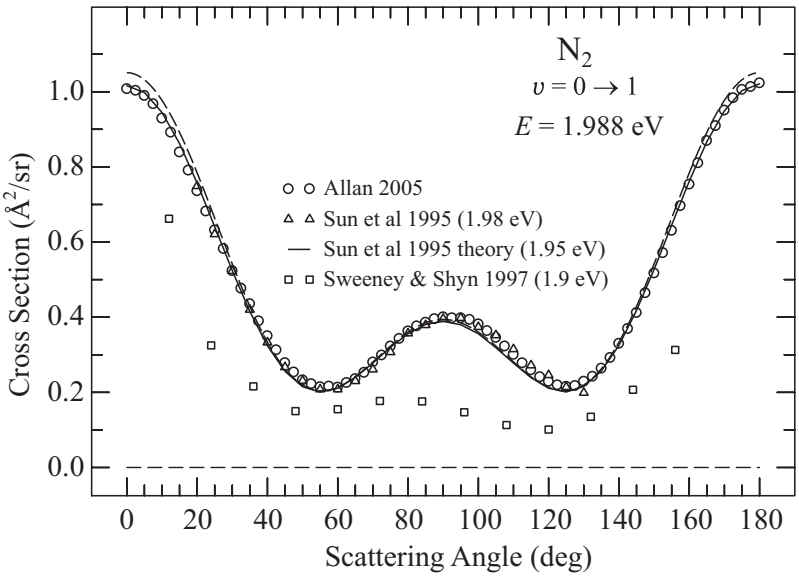

Figure 1.9: Rotationally summed $v = 0 \rightarrow 1$ cross section at $E = 1.988$ eV. The results of Sun et al. 1995, Sweeney and Shyn 1997 and the d_π wave distribution (dashed line, normalized to the experiment at 90°), are shown for comparison. Reprinted with permission from M. Allan, Measurement of the elastic and $v = 0 - 1$ differential electron-N_2 cross sections over a wide angular range. J. Phys. B: At. Mol. Opt. Phys. 2005 **38**, 3655-3672. Copyright 2005 IOP Publishing Ltd.

in the resonance region. The difference becomes larger below about 30° at 1.94 eV. The data of Jung et al. 1982 (open triangles in Fig. 1.10) agree very well with the present data in shape, but are slightly higher in magnitude. The angular distribution in the resonance region, at 1.94 eV in Fig. 1.10, is nearly symmetric around 90°, with the exception of a peak at 0°. It is dramatically different from that of N_2, shown in Fig. 1.9.

Poparić et al. 2004 measured the ratio of the forward and backward cross sections in the resonance region to be 1.00 ± 0.06, in an apparent contradiction to the data in Fig. 1.10, which has a forward peak. The two measurements are probably not contradictory, however, the difference could be a consequence of the fact that the magnetically collimated spectrometers such as used by Poparić et al. have a wide acceptance angle at low energy (Asmis and Allan 1997b) and are thus insensitive to a narrow peak at $\theta = 0°$.

Angular distributions such as those in Fig. 1.10 were multiplied by $2\pi\sin\theta$ and integrated to obtain integral cross sections. Examples of the ICSs obtained in this way are given, as empty circles, in Fig. 1.11 for the elastic scattering and in Fig. 1.12 for $v = 1$ excitation. The detailed shape of the cross section as a function of energy is then obtained as a weighted sum of several differential cross sections measured at several angles. These sums are shown as solid lines in Figs. 1.11 and 1.12. They are in excellent agreement with the integral cross sections of Gibson et al. 1996 for the elastic cross section and are about 20% higher for the $v = 1$ cross section.

In the resonance region there is an excellent agreement with the calculated cross section of Morgan 1991, both in terms of shape and in terms of absolute value. Below

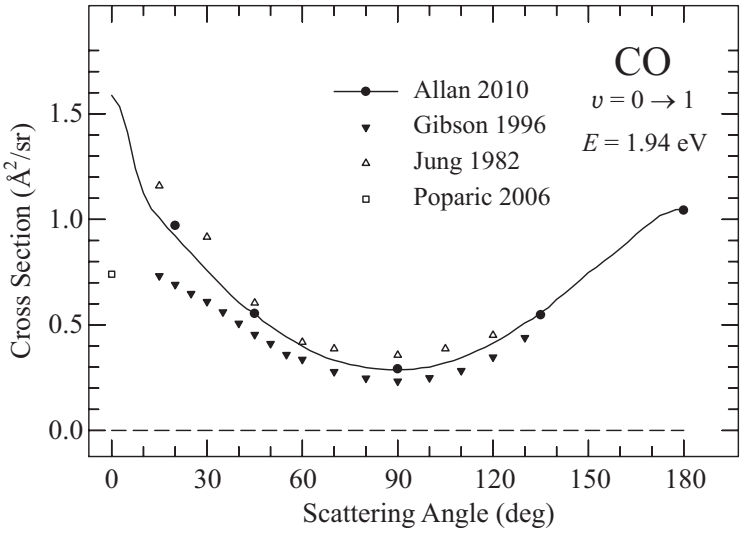

Figure 1.10: Angular distribution of electrons having excited the $v = 1$ level of CO at the peak of the $^2\Pi$ resonance. The data of Gibson et al. 1996, Jung et al. 1982 and of Poparić et al. 2006 are compared to that of Allan 2010. Redrawn from Allan 2010.

the resonance region, the present cross section is in reasonable agreement with that of Sohn et al. 1985. It is, however, nearly twice as high as the cross section derived from transport phenomena by Hake and Phelps 1967. This discrepancy between swarm and beam data was already noted by Schulz 1973, and Sohn et al. 1985.

Integral cross sections up to $v = 11$ were obtained in a similar way and used to construct the grand total cross section as the sum of the partial integral cross sections, as shown in Fig. 1.13. This test is important because the grand-total cross sections were measured in transmission-type experiments, which do not have many of the problems encountered in the measurement of partial differential cross sections, in particular the correction for instrumental response functions, or use of the relative flow method. The result is very satisfactory, the present sum agrees very well with the grand total cross sections of Szmytkowski et al. 1996 and of Buckman and Lohmann 1986. The experiment of Kwan et al. 1983, optimized for positron scattering, yielded cross sections which are larger at energies below 2 eV, but the problem is presumably only a small offset of the energy scale, by about 0.15 eV. The accuracy, and the low-energy capacity, of the 1930 data of Ramsauer and Kollath 1930 is remarkable in view of the simplicity of the equipment available at the time.

1.5 Hydrogen halides

The two molecules discussed in the preceding chapters, N_2 and CO, had π^* resonances coupled to d or p waves, resulting in a substantial centrifugal barriers and autodetachment widths Γ smaller but comparable to the vibrational spacing. This leads to the well-known boomerang structure (Birtwistle and Herzenberg 1971, Dubé and Herzenberg 1979, Schulz 1973).

Oscillatory structures were found in a number of resonances where the autodetachment

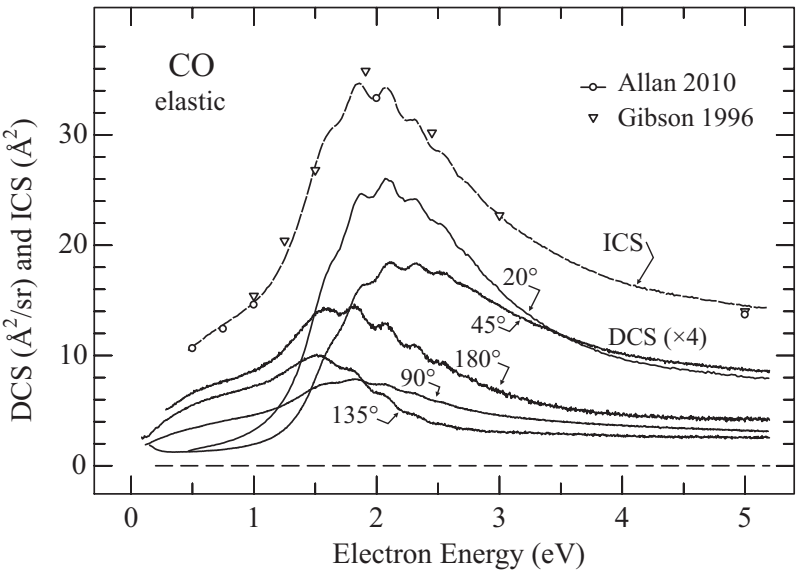

Figure 1.11: Integral elastic cross sections obtained by integration under the angular distributions are shown as circles (Allan 2010). The top (dashed) curve shows the shape of the ICS, obtained as a weighted sum of the differential cross sections, shown for comparison below the ICS (4× vertically expanded). The data of Gibson et al. 1996 is shown as triangles. Reprinted with permission from M. Allan, Electron collisions with CO: Elastic and vibrational excitation cross sections. Phys. Rev. A 2010 **81**, 042706/1-9. Copyright 2010 American Physical Society.

width is much larger than the vibrational spacing, however, and Fig. 1.14 shows several examples. The halogen halides show a second interesting feature - threshold peaks in the excitation of certain vibrational states. The threshold peaks are absent in H_2 and are related to the dipole moment (and polarizability) of the hydrogen halides.

Both features were studied a number of times. The oscillations in the excitation of high vibrational levels of H_2 were predicted by Mündel et al. 1985 and experimentally confirmed by Allan 1985. The oscillations in the $v = 1$ cross section of HCl were reported experimentally by Cvejanovic and Jureta 1989 and predicted independently by Domcke 1989. The experiment was confirmed by Schafer and Allan 1991 and a high resolution experimental study accompanied by nonlocal resonance model calculations was presented by Allan et al. 2000. The structures in HF were important in that they were the first positive experimental identification of vibrational Feshbach resonances (Knoth et al. 1989), called 'nuclear excited resonances' in older literature. They were studied up to high vibrational levels and with high resolution, accompanied by nonlocal resonance theory, by Sergenton et al. 2000 and Čížek et al. 2003. A high resolution experimental study and nonlocal model calculations for HBr and DBr were reported by Čížek et al. 2001. The subject of threshold peaks was reviewed by Cvejanović 1993. The discovery of pronounced threshold peaks in the vibrational excitation (VE) cross sections of HF, HCl and HBr by Rohr and Linder 1975, Rohr 1978 has initiated intense experimental and theoretical research on low-energy collisions with hydrogen halides. A survey of the experimental de-

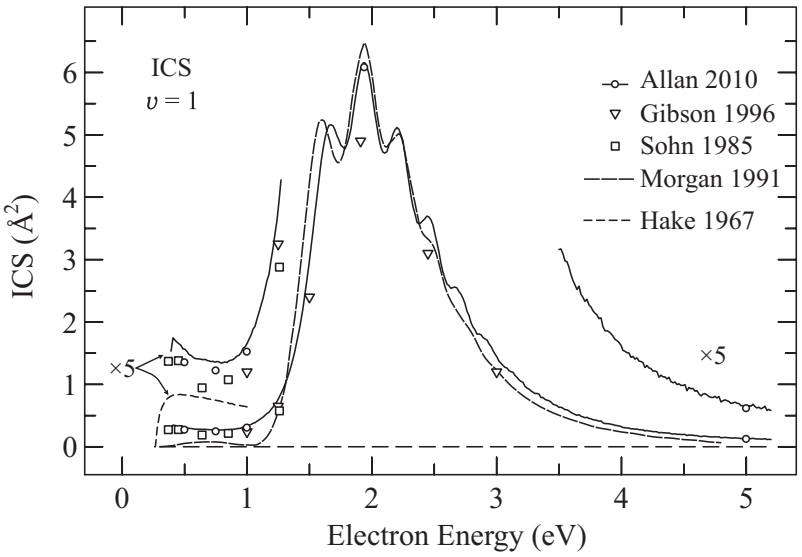

Figure 1.12: As Fig. 1.11, but for excitation of $v = 1$. Also shown is the data of Gibson et al. 1996, Sohn et al. 1985, Hake and Phelps 1967 (from drift velocity measurements, shown 5× vertically expanded), and Morgan 1991 (theory). Reprinted with permission from M. Allan, Electron collisions with CO: Elastic and vibrational excitation cross sections. Phys. Rev. A 2010 **81**, 042706/1-9. Copyright 2010 American Physical Society.

velopments has been given by Cvejanović 1993. The theoretical developments have been reviewed by Fabrikant 1990, Domcke 1991 and Horáček 2000. Various experimental and theoretical aspects of threshold phenomena were reviewed by Hotop et al. 2003.

The understanding of the observed phenomena, which emerged from the nonlocal resonance theory, can be rationalized using the schematic potential curves shown in Fig. 1.15. At large internuclear distances R the electron is captured in an antibonding valence σ^* orbital. This reduces the bond order to 0.5 and the curve's minimum is shallower and at a larger R than that of the neutral molecule. A second potential curve arises in the hydrogen halides (but not H_2) from the binding of the incident electron by the dipole moment of the molecule. This binding decreases with decreasing R as the dipole moment decreases and the dipole bound potential curve disappears below a critical R. An avoided crossing smoothly joins the valence and the dipole bound curves to yield the adiabatic potential curve. The dipole-bound branch of the potential curve supports Vibrational Feshbach resonances (VFRs) because, classically speaking, as the nuclei oscillate in the presence of the incident electron, they allow the electron cloud to leave at short R, but before it can leave completely, it is partly recaptured when the nuclei return to larger R where the dipole moment is larger (Gauyacq 1987). The VFRs are narrower and only slightly below the parent vibrational state for low v, and become broader and further below the parent state for larger v. At higher v is the outgoing nuclear wave packet reflected not by the dipole-bound branch of the potential curve, but by the valence part, at a much larger R. The corresponding resonant states are consequently much closer spaced and a rela-

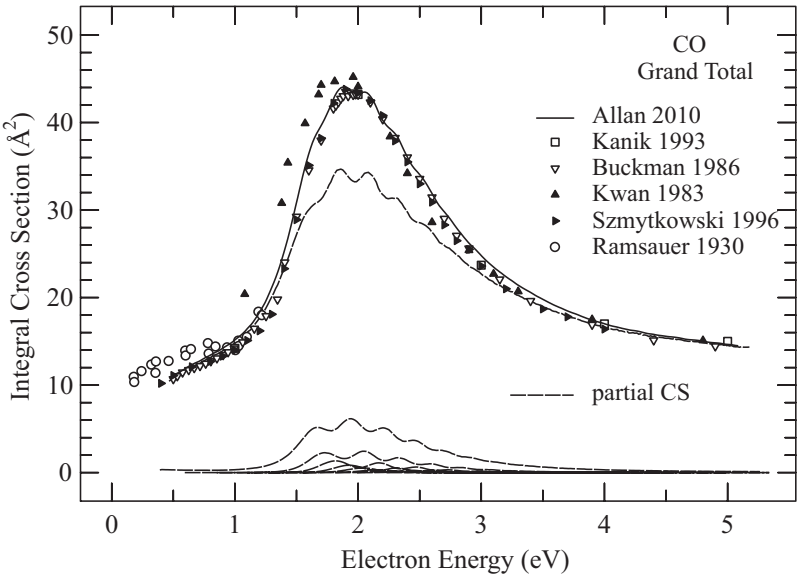

Figure 1.13: Grand total cross section. The results of Ramsauer and Kollath 1930, Buckman and Lohmann 1986, Kwan et al. 1983, Szmytkowski et al. 1996, as well as the 'recommended' data of Kanik et al. 1993 are shown for comparison. The present elastic and vibrational excitation integral cross sections are also shown. Reprinted with permission from M. Allan, Electron collisions with CO: Elastic and vibrational excitation cross sections. Phys. Rev. A 2010 **81**, 042706/1-9. Copyright 2010 American Physical Society.

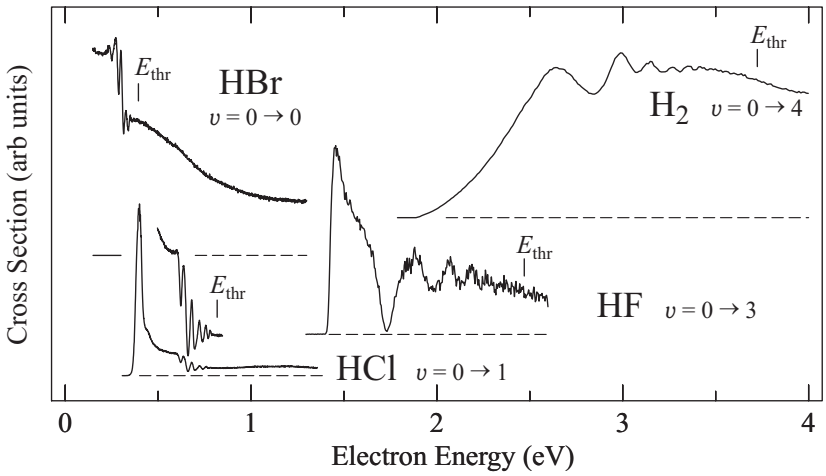

Figure 1.14: Selected cross sections of halogen halides and H_2 illustrating the common features, in particular oscillatory structures converging to the DEA threshold (marked as E_{thr}).

tion to specific parent vibrational levels is no longer meaningful – boomerang oscillations converging to the DEA threshold are observed.

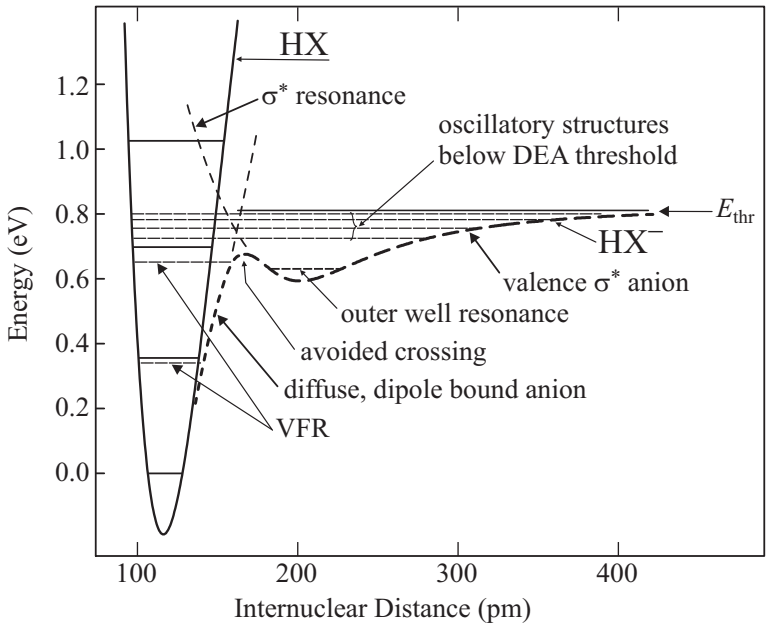

Figure 1.15: Generic potential curves illustrating the phenomena encountered in halogen halides. They are based in the theoretical findings of the nonlocal resonance theory, see for example Čížek et al. 2002 and references therein, and Fig. 5.5 of chapter 5 of this book.

The influence of a VFR, situated below its parent vibrational level, extends even above the parent level and increases the cross section for its excitation – it causes a threshold peak. Depending on the position of the avoided crossing and the minimum of the valence curve for a given molecule the adiabatic potential curve may or may not have outer well. No outer well was found for HF, but it was found for HCl, where it gives rise to narrow 'outer well resonances' (Allan et al. 2000). A (virtual state) cusp in the cross section is observed in the cross sections when the dipole (and polarizability) binding is not strong enough to support a VFR. Fabrikant (Hotop et al. 2003) nicely demonstrated how does the appearance of the cross sections depend on the molecular properties, on a model case with adjustable dipole moment and polarizability – going from a virtual-state cusp to a sharp VFR as the polarizability increases.

The various resulting experimental features, and in particular the coupling between the various channels, are illustrated in Fig. 1.16 on the example of HBr. The energy-loss spectrum shown on the top visualizes the vibrational thresholds. The elastic cross section has a downward step (a cusp) at the $v = 1$ energy and, superimposed on it, boomerang oscillatory structure converging to the DEA threshold (labeled E_{thr}). (The downward step and the boomerang oscillations become separated in energy, and thus visible as two different entities, in DBr (Čížek et al. 2001).) The $v = 0 \rightarrow 1$ cross section has a threshold peak, with barely visible oscillations superimposed on it (their visibility is better in DBr), and then step-like structures at higher vibrational thresholds, alternatively up and down. Finally, the DEA cross section has a peak at threshold and stepwise drops at vibrational thresholds, that is, when new vibrational excitation channels

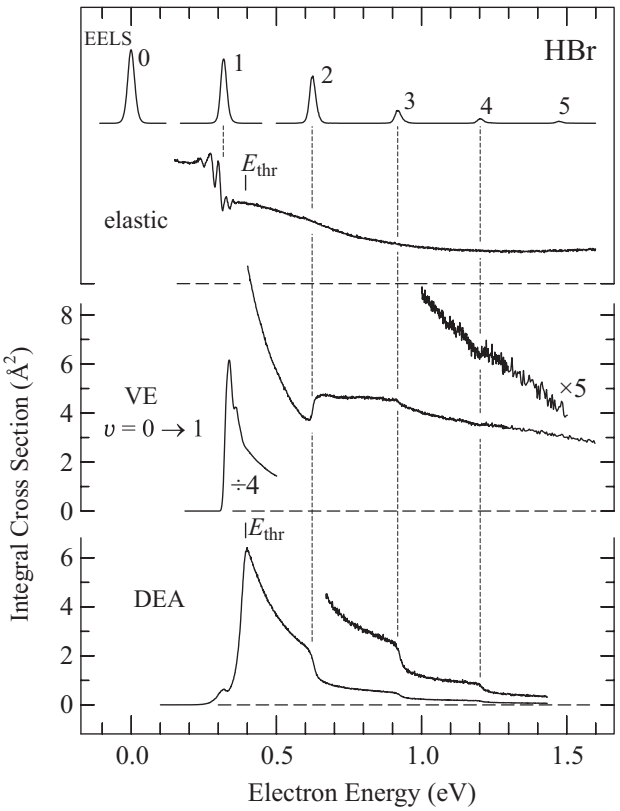

Figure 1.16: Comparison of the DEA, the VE and the elastic cross sections in HBr. An energy-loss spectrum (recorded at $\theta = 90°$ and $E_r = 0.5$ eV) is shown on the top to indicate the vibrational thresholds. (The data is mostly from Čížek et al. 2001.)

open. These steps were first reported in HCl by Abouaf and Teillet-Billy 1977 (see also Teillet-Billy and Gauyacq 1984) and in HBr by Abouaf and Teillet-Billy 1980.

The capacity of the nonlocal theory to reproduce the details of the shape of the DEA cross sections is illustrated in Fig. 1.17 (Čížek et al. 2001). High resolution absolute DEA spectra were obtained by recording their shapes under high resolution on the instrument with hemispherical analysers, where electron and ion signals were separated using the Wien filter built-in in front of the detector, and normalizing their magnitudes to absolute values measured later with the total ion collection instrument (Fedor et al. 2008). The agreement is very good, in particular in view of the fact that not only the shapes, but also the absolute magnitudes are compared. A similar agreement of magnitudes was recently obtained also for HCl, after the parameters of the nonlocal resonance model were improved by fitting into recent *ab initio* scattering calculation results (Fedor et al. 2010).

Figure 1.18 compares experiment and theory for vibrational excitation. The shape of the VE cross section was measured at 90° (Čížek et al. 2001). The absolute values were determined by the relative flow method at several angles, the angular distribution was measured at 2 eV and integrated to yield ICS (Allan 2007, unpublished). Absolute differential VE cross section was also measured at 90° and 1 eV and the average of these two

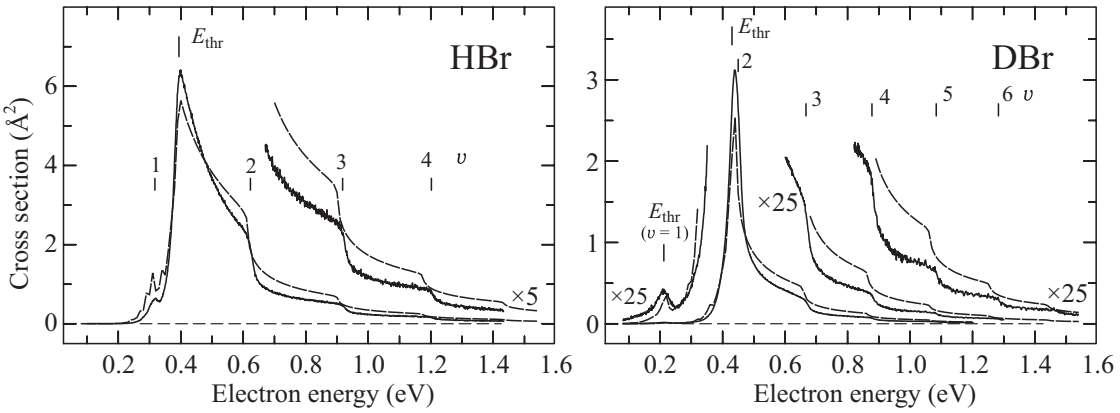

Figure 1.17: Comparison of the DEA cross sections for HBr and DBr. The dashed line shows the result of nonlocal resonant theory. (The theoretical data is from Čížek et al. 2001, experimental data from (Fedor et al. 2008).)

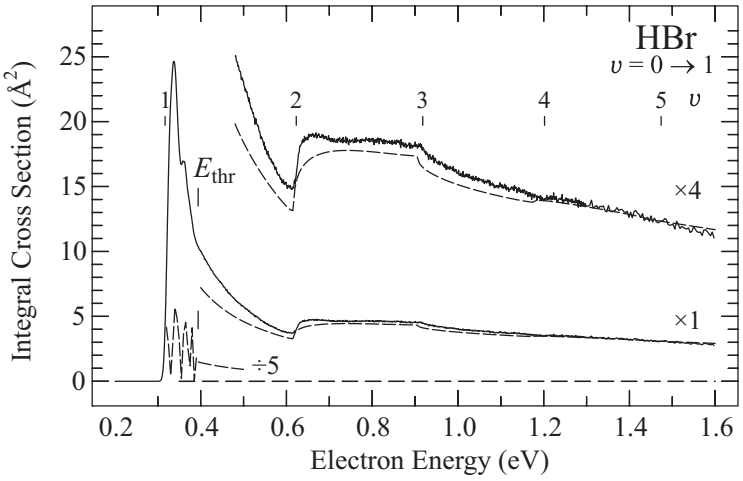

Figure 1.18: Integral experimental (solid line) and theoretical (dashed line) cross section for the excitation of $v = 1$ in HBr. The DEA threshold E_{thr} and the vibrational energies of neutral HBr are marked. (The data is from Čížek et al. 2001, but the experiment was normalized to absolute value in this work.)

normalizations is shown in Figure 1.18. The agreement in the magnitude and the details of the shape is excellent. Theory predicts very narrow oscillatory structure between the VE and the DEA thresholds, for which some evidence is seen in the experiment, as a shoulder. The visibility of this structure is better in DBr where the gap between the VE and the DEA thresholds is larger. Very good agreement of the shapes and structures in the VE and elastic CSs observed experimentally and calculated by the nonlocal resonance theory was obtained also for HCl (Allan et al. 2000, Čížek et al. 2002), although absolute values of the CSs are not yet available.

From the above discussion it follows that no threshold peaks and oscillations should occur above the DEA threshold and, in line with this expectation, no threshold peaks and oscillations were found in HI (Sergenton and Allan 2000), and in HCl for excitation of vibrational levels above the DEA threshold, $v \geq 3$ (Čížek et al. 2002).

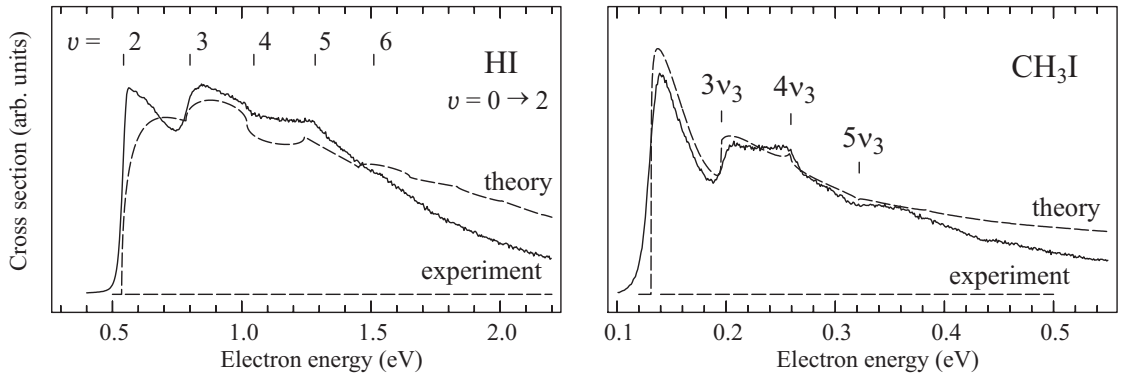

Figure 1.19: Cross sections for the excitation of two quanta of the H−I resp. H_3C−I vibrations in HI and CH_3I. Theory for HI is from Horáček et al. 1997. Figure on the left is reprinted from Chem. Phys. Lett. 2000, **319**, A.-C. Sergenton, M. Allan, Excitation of vibrational levels of HI up to $v = 8$ by electron impact, 179-183, Copyright (2000), with permission from Elsevier. Figure on the right is reprinted with permission from M. Allan, I. I. Fabrikant, Threshold peaks and structures in vibrational excitation of CH_3I by electron impact. J. Phys. B: At. Mol. Opt. Phys. 2002, **35**, 1025. Copyright 2002 IOP Publishing Ltd.

1.6 Methyl halides

Carbon has an electronegativity similar to that of hydrogen and one may thus expect a similarity of behavior when the hydrogen in hydrogen halides is replaced by a methyl. This class of compounds has been extensively studied – see for example (Hotop et al. 2003), and only one example will be shown here.

1.6.1 CH_3I

Figure 1.19 compares the VE cross sections (both experimental and theoretical) for a hydrogen iodide and methyl iodide. DEA is exothermic for both HI and CH_3I and this represents a major difference compared to the preceding cases of HCl and HBr. The potential curves of CH_3I were given by Hotop et al. 2003.

The shapes of the experimental curves are well reproduced by the nonlocal resonance theory (HI, Sergenton and Allan 2000) and the effective range R-matrix theory (CH_3I, Allan and Fabrikant 2002). The essential physics is clearly seen to be the same for both molecules, bearing out their chemical similarities. Neither curve has a clear threshold peak, because the entire spectra are above the DEA threshold. There are clear similarities between HI and CH_3I, and the shape of the part of the HBr cross section which lies above

the DEA threshold (Fig. 1.18), and with the HCl and HBr cross sections for exciting higher vibrational levels, those which lie above the DEA threshold. All these curves are characterized by steps at vibrational thresholds, alternately up and down (with the up and down behavior alternating also when the final vibrational quantum is incremented. The DEA cross sections for CH_3I were measured under ultrahigh resolution and calculated by Schramm et al. 1999 (see also the review by Hotop et al. 2003). The DAE cross sections for CH_3Cl and CH_3Br were calculated by Wilde et al. 2000, Gallup and Fabrikant 2007. These studies revealed further resemblance with HCl and HBr – the cross sections are characterized by the downward steps at vibrational thresholds caused by interchannel coupling. All these results confirm the prototype role played by the hydrogen halides.

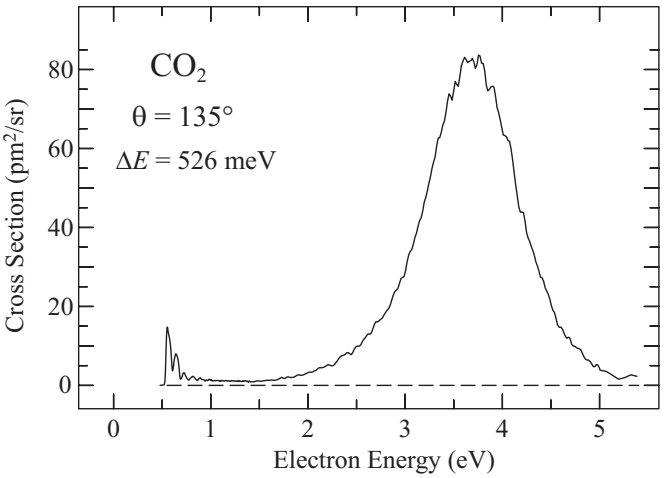

Figure 1.20: Cross section for exciting the topmost member of the Fermi polyad $\{(3,0,0),(2,2,0),\text{etc.}\}$, recorded at $\theta = 135°$ (Allan 2002, unpublished).

1.7 Vibrational Feshbach resonances without a permanent dipole

1.7.1 CO_2

Carbon dioxide has been studied many times and only representative references can be given here. CO_2 has no permanent dipole moment and one would therefore expect that it, unlike the hydrogen halides, does not have VFRs. It has long been known that intense vibrational excitation and DEA are caused by a $^2\Pi_g$ shape resonance centered at 3.8 eV (Boness and Schulz 1974). Large cross sections were found for certain vibrations even near threshold, and this cross section enhancement was ascribed to a virtual state (Morgan 1998, Estrada and Domcke 1985). The threshold peak did not have any structure, however, consistent with the notion that a virtual state does not involve any delay in the motion of electron. High resolution measurement revealed that the virtual state excites only the upper member of the $\{(1,0,0),(0,2,0)\}$ Fermi dyad (Allan 2001).

A subsequent study with higher sensitivity such as that shown in Fig. 1.20 revealed

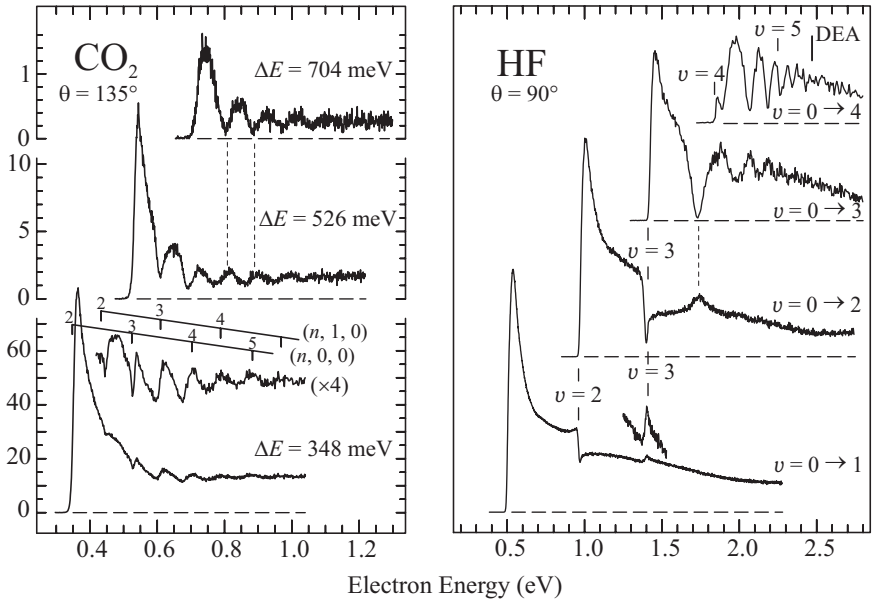

Figure 1.21: Comparison of the VE cross sections of HF and, in each case, of the topmost member of the Fermi polyad involving the bending and symmetric stretch vibrations of CO_2. (The label $(n, 0, 0)$ is meant to indicate, for example for $n = 2$, the topmost member of the Fermi polyad $\{(2, 0, 0), (1, 2, 0), (0, 4, 0)\}$.) (Allan 2002 ($CO_2$) and Čížek et al. 2003 (HF)) Figure on the left is reprinted with permission from M. Allan, Vibrational structures in electron-CO_2 scattering below the $^2\Pi_u$ shape resonance. J. Phys. B: At. Mol. Opt. Phys. 2002, **35**, L387. Copyright 2002 IOP Publishing Ltd. Figure on the right is reprinted with permission from M. Čížek, J. Horáček, M. Allan, I. I. Fabrikant, W. Domcke, Vibrational excitation of hydrogen fluoride by low-energy electrons: Theory and experiment. J. Phys. B: At. Mol. Opt. Phys. 2003, **36**, 2837-2849. Copyright 2003 IOP Publishing Ltd.

that only the topmost member of each Fermi polyad is excited by the virtual state at threshold, and narrow structure appeared on the threshold peaks. Similarly to the case of H_2 and many other VE cross sections, the boomerang and other structures appear more pronounced in the cross sections for higher-lying vibrational states. The threshold region of the cross sections for three higher-lying Fermi-coupled states are shown in Fig. 1.21. Many qualitative aspects of the structures are strikingly similar to those found in HF, shown for comparison on the right in the Figure. HF is the textbook case for VFRs, and the structures in CO_2 can thus also be assigned to VFRs. In both cases, the structures are shallower and narrower in the cross sections for the lower-lying final vibrational states, and become deeper and wider for the higher-lying final vibrational states. For each final vibrational state, the structures are narrower at lower energy and become wider with rising energy. There is an alternation in how the resonant contribution interferes with the nonresonant background – if a given VFR appears as a peak in the cross section for one final vibrational level, it will appear as a dip in final vibrational levels higher or lower by one. This relation is indicated by vertical dashed lines in the Figure. The threshold structures in CO_2 were qualitatively reproduced by Vanroose et al. 2004.

Qualitative potential curves in Fig. 1.22 rationalize and provide a physical picture for the observations. The curves for HF, adopted from the work of Čížek et al. 2003, are similar to the curves in Fig. 1.15, except that the outer well is not developed in HF. At low energies the nuclear wave packet is reflected on the dipole-bound outer wall of the potential, giving rise to the VFRs, which are deeper and deeper below the respective parent vibrational levels with rising v, as the potential well widens. At higher energies the wave packet is reflected on the valence-type outer wall, has to travel a long distance, the spacings of the oscillations become much narrower than the vibrational spacing of the neutral HF, and the concept of the parent vibrational state is no longer meaningful. The situation in CO_2 is similar, but with respect to the bending motion. The potential of (the lower branch of) the $^2\Pi_u$ shape resonance responsible for the 3.7 eV peak in Fig. 1.20 is known to descend, cross the potential of neutral CO_2, and be responsible for the 'outer well', supporting a metastable CO_2^-. This potential bends down before crossing the neutral, because of dipole and polarizability binding, similarly to the case of hydrogen halides. This view was supported by the high level electronic structure calculations of Sommerfeld 2003 and Sommerfeld et al. 2003 who have shown that the potential energy surface of the anion bends down before reaching the potential energy surface of the neutral CO_2.

Very sharp VFRs vere observed in the ultrahigh resolution experiments on CO_2 clusters by Barsotti et al. 2002 (see also Denifl et al. 2010). These VFRs were identified also in thin films, where they make a substantial contribution to electron trapping (Michaud et al. 2007).

1.8 Vibrational Feshbach resonances as doorway states to DEA

1.8.1 N_2O

Early studies of N_2O (for example that of Azria et al. 1975) revealed a structureless $^2\Pi$ shape resonance at 2.3 eV, which has also been studied theoretically, for example by Dubé and Herzenberg 1975 and Bettega et al. 2006. This resonance leads to O^- forma-

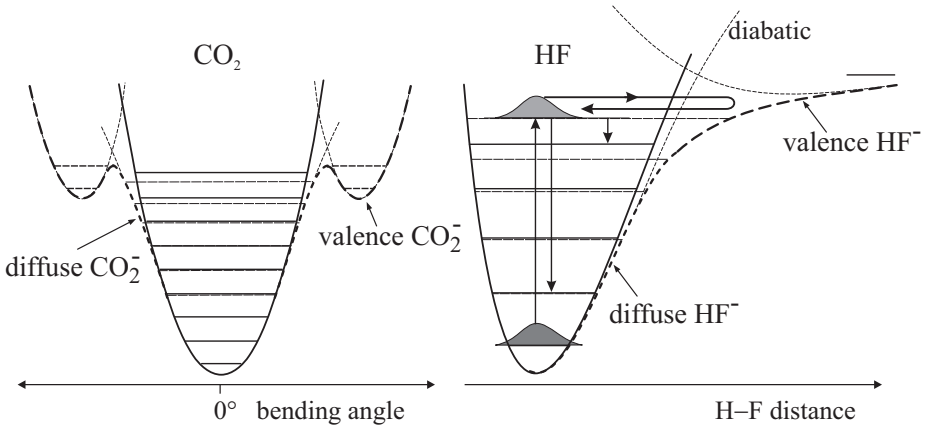

Figure 1.22: Qualitative potential curves for CO_2 and HF. The HF potential curves are based on those calculated for the nonlocal resonance model of Čížek et al. 2003, the CO_2 potential curves are hypothetical. Figure on the left is reprinted with permission from M. Allan, Vibrational structures in electron-CO_2 scattering below the $^2\Pi_u$ shape resonance. J. Phys. B: At. Mol. Opt. Phys. 2002, **35**, L387. Copyright 2002 IOP Publishing Ltd.

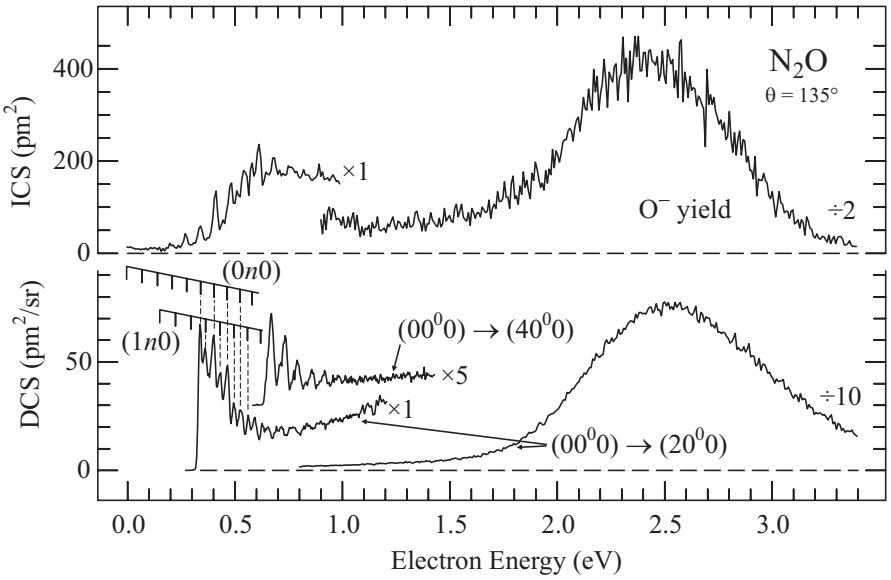

Figure 1.23: High resolution DEA (top) and vibrational excitation curves for N_2O. The data is from Allan and Skalický 2003.

tion at 2.3 eV, with a shoulder at low energies and the cross section was measured by Rapp and Briglia 1965, Chaney and Christophorou 1969, Krishnakumar and Srivastava 1990 and by May et al. 2008 with a good mutual agreement. Chantry 1969 and Chaney and Christophorou 1969 reported that the shoulder increases dramatically with temperature. Weber et al. 1999 discovered very narrow VFRs in N_2O clusters using the laser photoelectron attachment

method, later studied over a wider energy range by Vizcaino et al. 2010. The low-energy processes described here may also play a role in electron trapping by thin films of N_2O, found to occur at energies down to 0 eV (Michaud et al. 1997).

A study with higher resolution and sensitivity revealed threshold peaks in the VE cross sections, and very narrow structures were superimposed on these threshold peaks in the cross sections for excitation of higher vibrational levels (Allan and Skalický 2003). As an example, the excitation of two and four quanta of the N−O stretch vibration ν_1, are shown in the bottom part of Fig. 1.23. The structures were interpreted to have the same origin as in CO_2 (Fig. 1.21), to be due to VFR supported by a branch of the potential surface which bends down before crossing the potential of neutral N_2O because of dipole and polarizability binding of the incoming electron. The peaks form two progressions in the bending vibration ν_2, $(0n0)$ and $(1n0)$. The peaks appear about 5 meV below the vibrational thresholds, but this is within the error limit of the energy scale calibration, so that, within the error limit, the structures appear at the energies of the parent vibrational states. This is in contrast to the prototype case of VFR, HF, shown in Fig. 1.21, where the higher VFRs are clearly seen to be below the parent vibrational levels.

A consequence of the weak N−O bond is that the threshold for DEA is only $E_{\rm thr} = 0.21$ eV. Since Fig. 1.21 shows that VFRs are supported by the bending motion up to an energy of about 0.9 eV, much higher than $E_{\rm thr}$, N_2O is a suitable case where one can study whether VFRs lead to dissociation, that is, whether they act as doorway states to DEA. The O^- yield was therefore measured under high resolution with the same instrument as the VE cross sections, the result was normalized to the absolute value of May et al. 2008, and is shown in the upper part of Fig. 1.23. Sharp structures are observed at the low-energy end of the spectrum, corresponding to the same progressions as those in the (20^00) excitation. These peaks represent a direct indication of the VFR acting as doorway states. The positions of the peaks are about 10 meV under the peaks in the VE cross sections, but this is within the error limit of the energy scale calibration.

N_2O is a suitable prototype case for the relaxation of VFRs into the dissociation channel, because the small size of the molecule makes the vibrational structure simple and well resolved, and because the VFR are observed in the two competing channels, VE and DEA. VFRs have were discussed as intermediates in DEA in several cases, in particular for biomolecules (Abouaf and Dunet 2005, Sommerfeld 2008, Burrow et al. 2006, Scheer et al. 2005, Sommerfeld 2007, Fabrikant 2009, Gallup and Fabrikant 2011). It is remarkable that VFRs are dominant intermediates in positron annihilation (Gribakin et al. 2010).

1.9 π^* shape resonances as a doorway states to DEA

1.9.1 Chlorobenzene

DEA to chlorobenzene (referred to as PhCl) has been studied many times. In this section we report on the insight gained by the comparison of vibrational excitation cross sections (in particular their selectivity) with a high resolution DEA spectrum, as presented by Skalický et al. 2002 (who also listed references to earlier DEA work).

Excitation of the ring breathing mode, shown on the left in Fig. 1.24, reveals a broad structured band in the 0.7-1.5 eV range which was assigned to two π^* shape resonances with temporary occupation of the orbitals shown on the right in the figure. The narrow

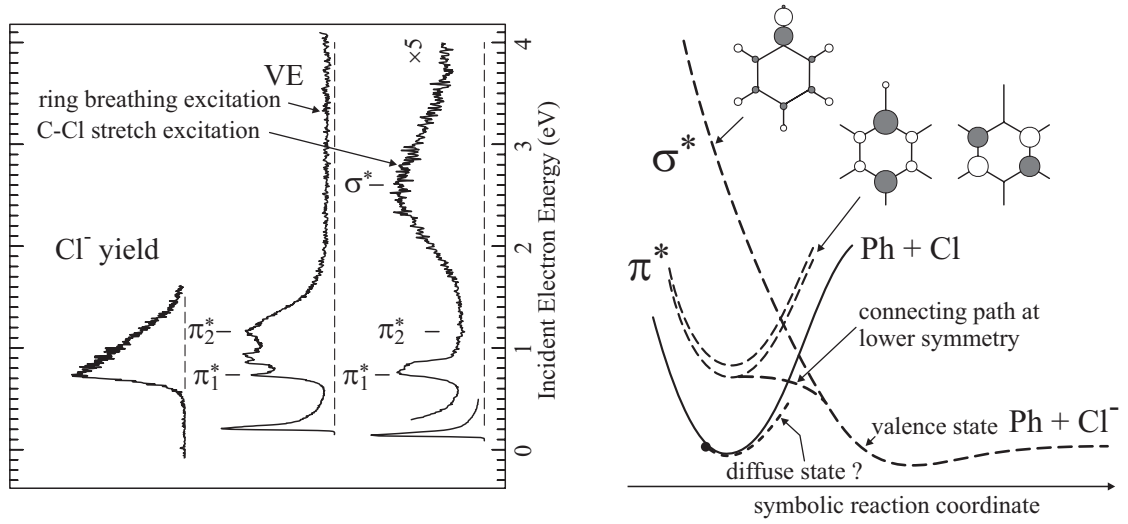

Figure 1.24: Left: Cross sections for VE and DEA in chlorobenzene. Right: Schematic potential curves and temporarily occupied orbitals. (Data is from Skalický et al. 2002.)

structure on the band indicates an autodetachment width of below 30 meV. The large width of the entire band must thus be due to Franck-Condon width and the fact that the Cl substituent lifted the degeneracy of the two π^* orbitals of benzene, as indicated by the labels π_1^* and π_2^*. The theoretical treatment of Skalický et al. 2002, using the very simple method of estimating energies of shape resonances by empirical scaling of SCF virtual energies, revealed dramatic vibronic coupling in the chlorobenzene anion so that the π_1^* and π_2^* resonances are highly mixed, with very complex potential surfaces.

Excitation of the C−Cl stretch mode reveals an additional broad unstructured band at 2.6 eV. The selectivity of the VE indicates that it is a σ^* resonance with temporary occupation of the σ^* orbital shown on the right in the figure (note that the π^* orbitals have a node in the plane of the paper, σ^* orbital does not). This assignment agrees with that of Stricklett et al. 1986, based on electron transmission spectroscopy (ETS).

Excitation of both vibrational modes has an intense threshold peak, but its origin is not certain. It could be a threshold peak due to dipole and polarizability binding, analogous to the threshold peaks in HBr discussed in the preseding section. But it could simply be due to direct excitation of IR active vibrations. This peak does not have any structure resembling that of the hydrogen halides or CH_3I.

The DEA spectrum was recorded with high resolution (about 10 meV) with the same instrument with hemispherical analyzers as the VE cross sections, using the Wien filter to separate ion and electron signals. An important observation is that the onset of the Cl^- signal is nearly vertical, about as steep as the VE cross section, and peaks at the same energy as the sharp $v = 0$ level of the π^* shape resonance, 0.73 eV. This indicates that the π^* resonance acts as a doorway state for DEA and dissociates without activation energy. The Cl^- formation can certainly not be a consequence of direct vertical electron capture into the σ^*_{C-Cl} resonance, which peaks at much higher energy. In fact, direct vertical electron capture into the σ^*_{C-Cl} orbital does not yield any Cl^- signal – the autodetachment

width is too large. The Cl^- formation can also not follow the mechanism for which the hydrogen halides are a prototype - this mechanism leads to a vertical fragment ion onset at the DEA threshold, and the Cl^- signal onset is 0.22 eV above threshold (the threshold energy is 0.5 eV, Bulliard et al. 1994).

This indicates that the presence of a π electron system has a profound influence on DEA by offering a doorway state which dominates the process. The absence of an activation barrier is not trivial because the dissociation in C_{2v} symmetry is forbidden. It is due to symmetry-lowering, a consequence of vibronic coupling. The work of Skalický et al. 2002 indicates that the symmetry-lowering involves the expected out-of-plane bending of the C−Cl bond, but also a less expected out-of-plane bending of the hydrogen atoms.

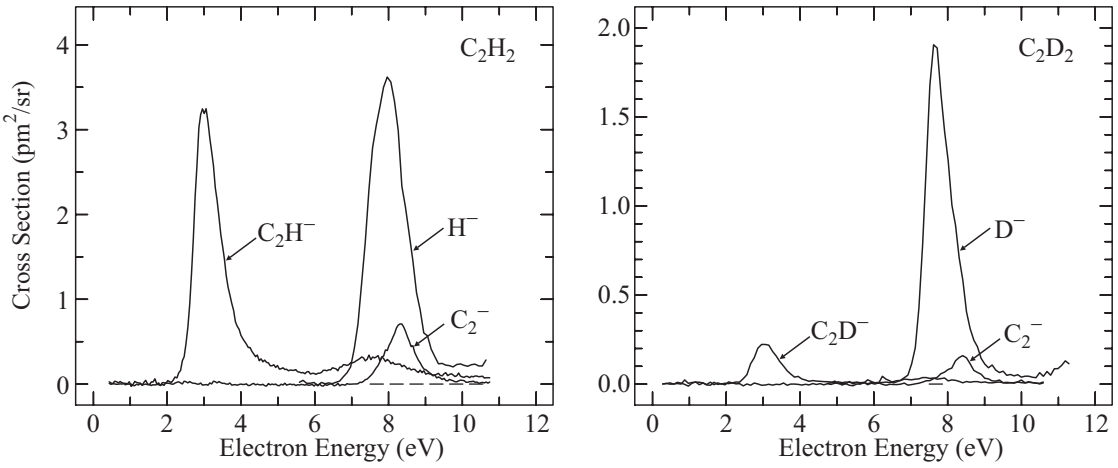

Figure 1.25: DEA cross sections for acetylene (left) and dideuteroacetylene (right). The data is from May et al. 2009.

1.9.2 Acetylene

Another example where a π^* shape resonance acts as a doorway state is acetylene. A relative DEA spectrum was given for example by Dressler and Allan 1987. The absolute cross sections were measured by Azria and Fiquet-Fayard 1972, Abouaf et al. 1981 and May et al. 2008. The isotope effect was found to be large, the DEA cross section of the deuterated compound being 15× smaller (May et al. 2009). Vibrational excitation was studied by Andrić and Hall 1988.

The theory of Chourou and Orel 2008 and of Chourou and Orel 2009a, which was refined to take into account the finite temperature of the sample, essential even at room temperature (Chourou and Orel 2009c), reproduced well the isotope effect, and the absolute magnitude was reproduced better than within a factor of two – a good agreement in view of the steep dependence on the primary results of the calculation, the resonance energy and width. An important achievement of the theory (which is validated by the agreement with the experiment) is the insight which it provides into the mechanism of the dissociation. It shows that the nuclear wave packet, to by-pass an energy barrier, needs first to move along the bending coordinate before it can dissociate (Chourou and Orel 2008). The

fundamental principle is thus the same as in the case of chlorobenzene in the preceding section.

In this respect it is interesting to observe that the same theoretical treatment, applied to the related case of HCN and DCN, revealed that, although the potential surface has a barrier in the dissociation path which can be by-passed by bending, like in the acetylene case, the system prefers to tunnel through the barrier instead of going around it (Chourou and Orel 2009b). The agreement with experiment (May et al. 2010) was slightly less good than in the acetylene case, but still qualitatively correct.

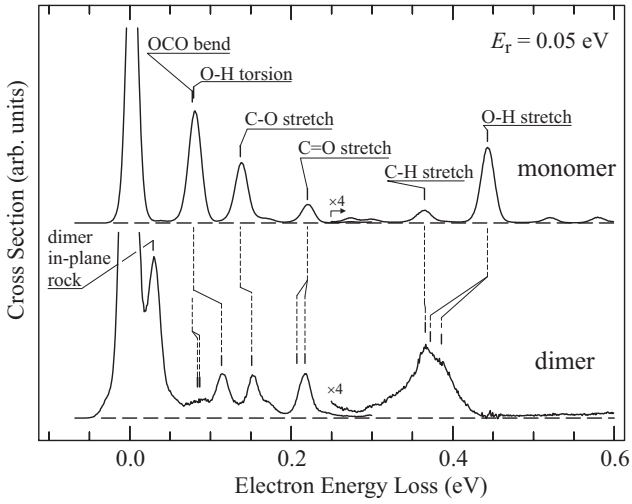

Figure 1.26: Electron energy-loss spectra of the monomer and the dimer of formic acid (Allan 2007b). Reprinted with permission from M. Allan, Electron collisions with formic acid monomer and dimer. Phys. Rev. Lett. 2007 **98**, 123201. Copyright 2007 American Physical Society.

1.10 OH and SH containing molecules

1.10.1 Formic acid

This section reviews the VE cross sections of the formic acid monomer (Allan 2006) and dimer (Allan 2007b) and discusses their implications on the resonant structure, nuclear dynamics, and DEA.

Targets with low and high concentrations of the dimer were obtained by expanding from either low pressure (through a 250 μm dia nozzle) or high pressure (through a 30 μm dia nozzle) gas. Pure dimer and monomer spectra were then obtained by minor spectra subtraction. The validity of the procedure was verified by the energy-loss spectra shown in Fig. 1.26. The very low frequency in-plane rock vibration identifies the dimer, and its absence indicates a pure monomer.

The cross sections for the excitation of the C=O stretch vibrations, shown in Fig. 1.27 identify the shape resonances. The 1.9 eV π^* resonance (studied theoretically by Gianturco and Lucchese 2004) of the monomer is split by 0.56 eV in the dimer and its

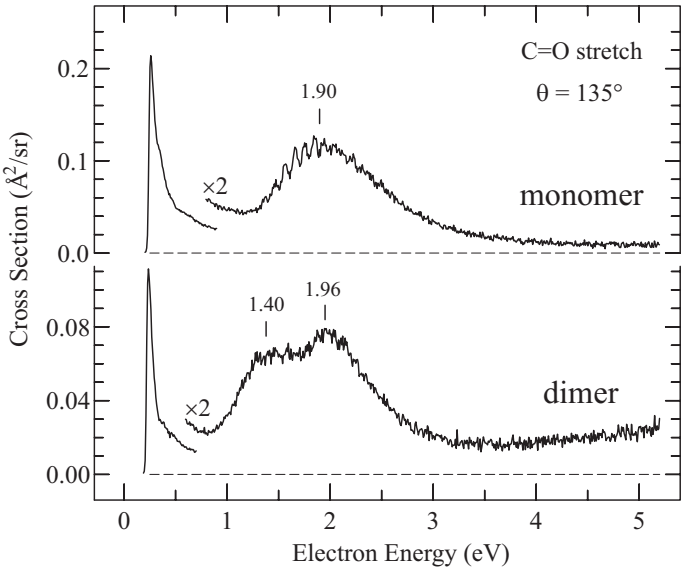

Figure 1.27: Cross sections for the excitation of the C=O stretch vibrations for the monomer and the dimer of formic acid (Allan 2007b). Reprinted with permission from M. Allan, Electron collisions with formic acid monomer and dimer. Phys. Rev. Lett. 2007 **98**, 123201. Copyright 2007 American Physical Society.

center shifts slightly down. The splitting is quite large in view of the fact that the two C=O bonds are not directly conjugated in the dimer and the interaction happens over a large distance. It is an experimental indication of the large spatial extend of the temporarily occupied orbitals. The cross section is slightly smaller in the dimer, presumably because the temporarily captured electron is distributed over many bonds, and affects each of them less. The two π^* resonances of the dimer were calculated qualitatively correctly by Gianturco et al. 2005, although both the absolute energies and their splitting were larger than the experimental values. The threshold peak of the dimer is smaller than that of the monomer, presumably because of the lack of a permanent dipole moment.

The π^* resonance seen in the C=O and C−H stretch excitation in Fig. 1.28 has boomerang structure associated with the OCO bending motion. This structure is barely visible in the O−H stretch excitation. The C=O stretch cross section has a high narrow threshold peak, but without structure. The peak is much lower in the C−H stretch cross section, presumably because this bond is much less polar.

An interesting question is whether there is resemblance between the O−H stretch cross sections of formic acid in Fig. 1.28 and the VE cross sections of hydrogen halides in Figs. 1.14, 1.16, 1.18 and 1.21. This may be expected because the hydrogen atom is bound to an electronegative atom in both cases, and both classes of compounds are acidic. Inspection of the spectra reveals a clear similarity in terms of a threshold peak and step-wise drops and rises of the cross section at vibrational thresholds. There is no oscillatory structure converging to the DEA threshold (at 1.37 eV), however.

In this sense the proposition of Gallup et al. 2009a (see also Fabrikant 2010) that also DEA follows the same mechanism is justified. Their nonlocal R-matrix calculation

was very successful in reproducing step-wise drops in the DEA cross section observed in the related molecule of glycine in the high resolution study of Abouaf 2008, which are interpreted as having the same origin as those shown in Fig. 1.17 for HBr. The description of this important feature, due to interchannel coupling, requires a nonlocal theory which is not yet available for more than one dimension, unfortunately. The possible role of the π^* resonance, shown by Rescigno et al. 2006, Rescigno et al. 2007 to spontaneously distort out of planarity to permit dissociation in a way similar to chlorobenzene and acetylene presented above, thus needs further investigation. The two approaches led to a lively discussion in the literature (Rescigno et al. 2009, Gallup et al. 2009b).

Step-wise structure was also reported in formic acid by Pelc et al. 2002 albeit not as pronounced as in glycine. Other DEA studies of formic acid were reported by Pelc et al. 2002, Pelc et al. 2003, Martin et al. 2005, Pelc et al. 2005 and Prabhudesaia et al. 2005.

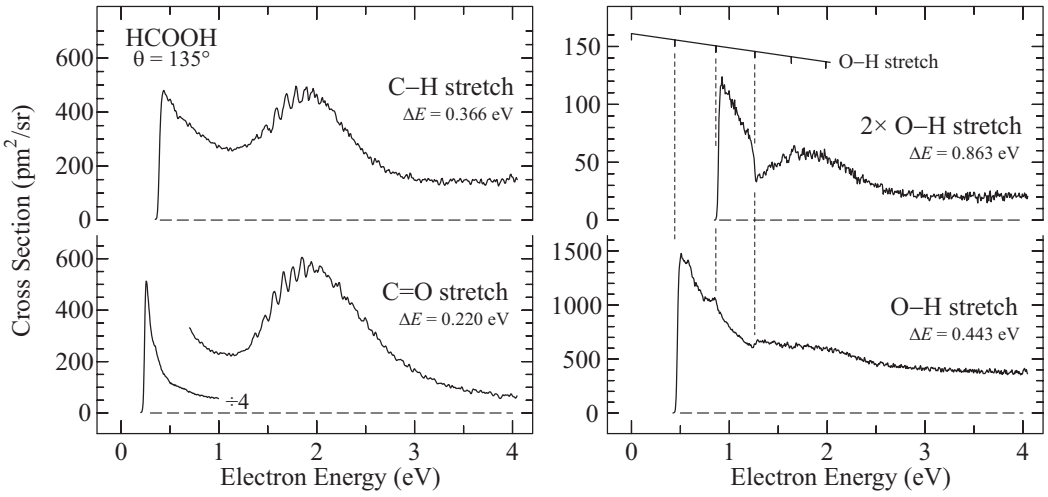

Figure 1.28: Cross sections for vibrational excitation of formic acid monomer. (Data from Allan 2006)

Intramolecular proton transfer driven by the attachment of an electron into the π^* resonance carries its experimental signature as a yield of slow electrons, visible in Fig. 1.29 (Allan 2007b). The species resulting from it, an ion-dipole complex of the formate anion and the protonated formic acid radical, and the reaction leading to it were studied theoretically by Bachorz et al. 2005. Proton-transferred complexes of formic acid with various biomolecules have also been generated in a high-voltage discharge ion source, mass selected, and studied by anion photoelectron spectroscopy – see for example the study with 1-methylcytosine (Ko et al. 2010).

1.10.2 Ethanol and thioethanol

Alcohols and thioalcohols are chemically related to the hydrogen halides in the sense that a hydrogen is bonded to an electronegative atom in both. Alcohols and thioalcohols are also acidic, but in contrast to the hydrogen halides only very weakly so. An interesting question is whether alcohols and thioalcohols show some of the phenomena described above

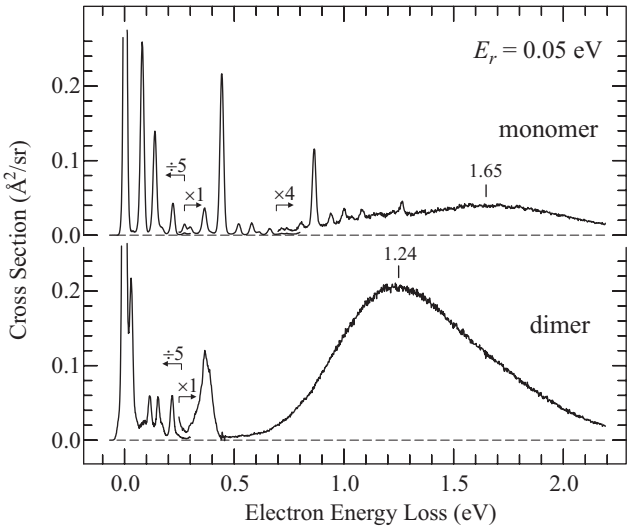

Figure 1.29: Energy loss spectra, recorded at a constant and very low residual energy, of formic acid monomer and dimer. The yield of low energy electrons from the dimer is about 20× larger from the monomer (note that the pertinent section of the monomer spectrum is shown multiplied by 4). The slow electrons are interpreted as a consequence of an intra-dimer proton transfer. Reprinted with permission from M. Allan, Electron collisions with formic acid monomer and dimer. Phys. Rev. Lett. 2007 **98**, 123201. Copyright 2007 American Physical Society.

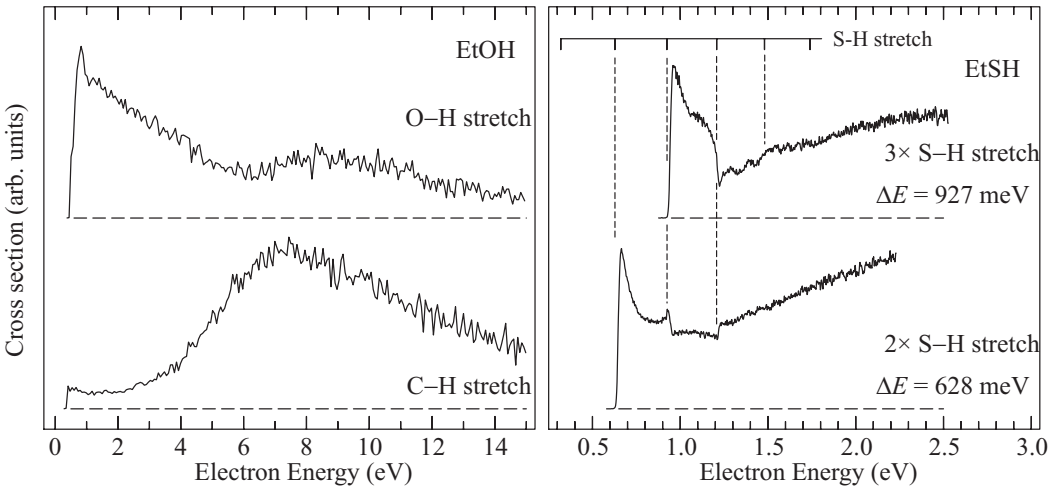

Figure 1.30: Cross sections for vibrational excitation of ethanol and thioethanol.

for hydrogen halides and formic acid.

Two (relative) VE cross sections were compared to DEA spectra by Ibănescu et al. 2007 and are reproduced in Fig. 1.30. The C−H stretch excitation cross section has a shape typical for VE cross sections in saturated hydrocarbons – with a peak around 8 eV and

low values below about 4 eV (Allan and Andrić 1996). The O−H stretch excitation cross section on the other hand is very different. It peaks at threshold and then decreases slowly over a large energy interval. This cross section enhancement is too broad to be due to direct dipole excitation – it must be due to a resonant process and could be due to a σ^* resonance combined with long range attraction by the dipole moment (1.68 D). There are no structures on the cross section, however, in contrast to hydrogen halides. The cross section for the excitation of two quanta of the O−H vibration is hard to measure because the cross section drops very rapidly with increasing quantum – an indication of a large autodetachment width of the resonance. The DEA cross section (not shown here) has a nearly vertical onset at the threshold energy, peaking at 2.75 eV (Ibănescu et al. 2007). The large isotope effect (4×) is another indication of a large autodetachment width.

Thioethanol resembles the hydrogen halides more, the excitation of high overtones of the S−H stretch vibration is pronounced and the spectra in Fig. 1.30 exhibit step-wise structures reminiscent of those in HBr or HF, taken to be consequence of long-range attraction. The principal difference to ethanol must be the higher polarizability, because the dipole moment is nearly the same (1.58 D). DEA, measured by Ibanescu and Allan 2009, yields two fragments at low energies. The $(M-H)^-$ fragment has a vertical onset at the threshold energy of 1.8 eV. The $(M-H_2)^-$ fragment has a vertical rise at the same energy of 1.8 eV, but in addition a puzzling structureless band with an onset near 0 eV, peaking at 0.6 eV.

1.11 Other polyatomic molecules

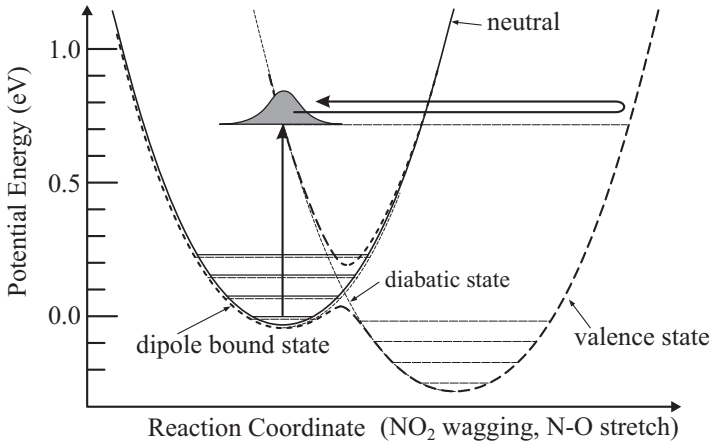

Figure 1.31: Schematic potential curves for nitromethane and its anion. Based on Sommerfeld 2002.

1.11.1 Nitromethane

Nitromethane is an interesting prototype case. Compton et al. 1996 studied nitromethane using the anion photoelectron spectra and Rydberg charge exchange. They recognized

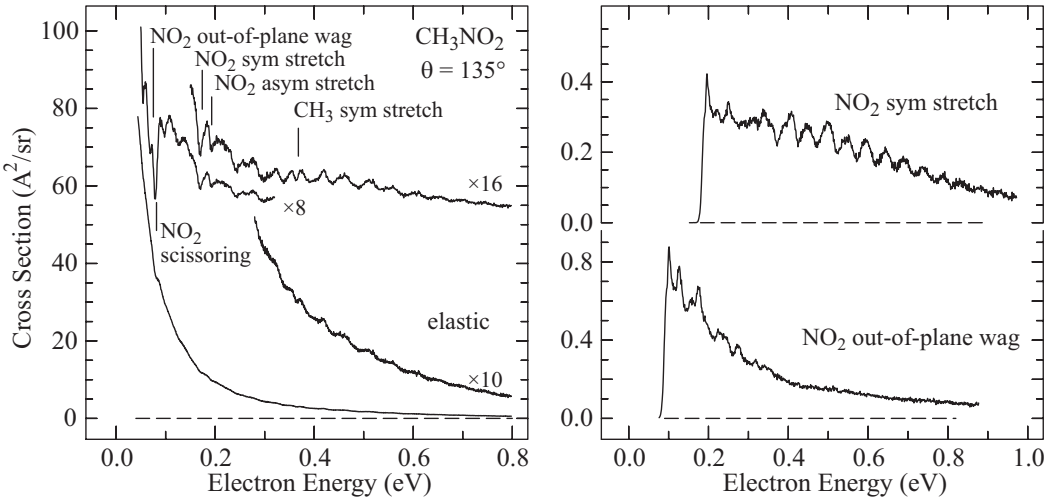

Figure 1.32: Left: Elastic DCS of nitromethane at 135°. The lower two curves are shown as recorded. Smoothly rising background was subtracted from the top two curves to enhance the visibility of the sharp structures. Energies of selected vibrations of neutral nitromethane are marked. Right: Cross sections for exciting the two vibrations indicated.

that Rydberg charge exchange leads to a dipole-bound state with an electron affinity of 12 ± 3 meV which serves as a doorway to a valence state of the anion with a substantially different structure and an adiabatic electron affinity of 0.26 ± 0.08 eV. The interconversion of the two states became evident in the study of Ar-solvated nitromethane anion of Lecomte et al. 2000. Dessent et al. 2000 observed the VFR in nitromethane in photoabsorption and photofragment action spectra of the $X^- \cdot CH_3NO_2$ ($X^- = I^-$ and Br^-) complexes, with peaks at the onsets of the $-NO_2$ wagging, scissoring, and stretch modes. Lunt et al. 2001 reported absolute total integral and total backward scattering cross sections from 30 meV to 1 eV and found them to increase rapidly with decreasing energy, but observed no structures. Absolute DEA cross sections were estimated experimentally by Sailer et al. 2002, who found NO_2^- to be the by far dominant fragment, with a peak cross section of 620 pm^2 at 0.62 eV. This low energy band appears to be absent in the ion desorption spectra from thin films (Bazin et al. 2009, Bazin et al. 2010).

Schematic potential curves of the two states were presented by Compton et al. 1996, and the experimental electron affinities were well reproduced by the high level *ab initio* calculations of Gutsev and Bartlett 1996. Sommerfeld 2002 (see also Sommerfeld 2008) presented high level *ab initio* calculations of both states and calculated the coupling matrix element between them to be 30 meV.

Schematic potential curves based on the theoretical work are presented in Fig. 1.31. Nitromethane has a supercritical dipole moment (3.46 D) and the dipole-bound state is therefore bound even at the equilibrium geometry of the neutral molecule, in contrast to the hydrogen halides shown in Figs. 1.15 and 1.22. The valence state of the anion has, relative to the neutral molecule, longer N−O bonds and it is pyramidal around the N-atom (Gutsev and Bartlett 1996). That means that the active path from the dipole-bound to the valence states is primarily along the symmetrical N−O stretch and the out-of-plane

NO_2 wagging modes.

An elastic and two representative inelastic cross sections, measured at 135° are shown in Fig. 1.32 (Allan 2004, unpublished). The elastic cross section is very large and rises rapidly at low energies, in agreement with the findings of Lunt et al. 2001. The visibility of the sharp structures is improved in the vertically expanded traces with a smooth background subtracted. The structure is dense and not all features can be uniquelly assigned, but sharp dips are evidently observed slightly below the energies of vibrations, which include those identified as important for the path between the dipole-bound and the valence states. (Vibrational frequencies were taken from Deak et al. 1999.) Experimentally the dips are 5 meV below the thresholds, which agrees with the dipole-bound electron affinity of 12 meV in view of the fact that the present energy scale calibration is reliable within ±20 meV. The structures become broader – boomerang oscillations – at energies around 0.5-0.7 eV. The cross section for exciting the NO_2 out-of-plane wagging vibration has sharp structures below 0.3 eV. The cross section for exciting the NO_2 symmetrical stretch vibration has sharp structures below 0.3 eV and broad boomerang oscillations in the 0.4-0.8 eV range. The sharp structures below 0.3 eV in all three cross sections are assigned to excited vibrational states of the dipole-bound anion (*i.e.*, to VFRs). Some of these states appear broadened, possibly by rapid interconversion into the valence state of the anion. The broad structures in the 0.4-0.8 eV range are assigned to a vertical attachment to the valence state, and boomerang oscillations on the (diabatic) potential of this state, as indicated by the horizontal returning arrow in Fig. 1.31. Motion on a diabatic potential is appropriate in view of, and supportive of, the theoretical conclusion of Sommerfeld 2002 that the nitromethane anion is clearly in the weak coupling regime, and any description of transitions between the dipole-bound and the valence state should be based on the diabatic picture.

It would be desirable to measure a high resolution study of DEA which would releave whether the VFR seen in the elastic and the VE cross sections also appear in the DEA spectrum.

1.11.2 Pyrrole

Pyrrole may serve as a simple prototype for the nucleobases and porphyrin, containing a hydrogen linked to a nitrogen in planar configuration in an unsaturated ring.

The cross section for excitation of the C=C and C−N stretch vibrations, shown in Fig. 1.33, reveals the two π^* shape resonances due to the temporary occupation of orbitals consisting essentially of the in-phase and out-of-phase combinations of the C=C π^* bond orbitals. The expected selectivity of vibrational excitation indicates that the two bands at 2.52 eV and 3.6 eV in the C=C and C−N stretch excitation are π^* resonances, and the 2.5 eV band in the N−H stretch excitation could be a N−H σ^* resonance predicted at about this energy by the scaled Koopmans model. The latter band could also be due to the π_1^* resonance – it has the same energy – although the hydrogen atom is in the nodal plane of the π_1^* orbital and would not be expected to be strongly effected by its occupation. Interesting is the cusp in the N−H stretch excitation cross section, at the energy of the $2\nu_1$ vibration, suggesting threshold phenomena related to those of the hydrogen halides. Note that this cusp is related to the N−H bond; it is absent in the C=C and C−N stretch cross section. DEA signal sets in at the threshold at 1.61 eV (derived from the gas phase acidity)

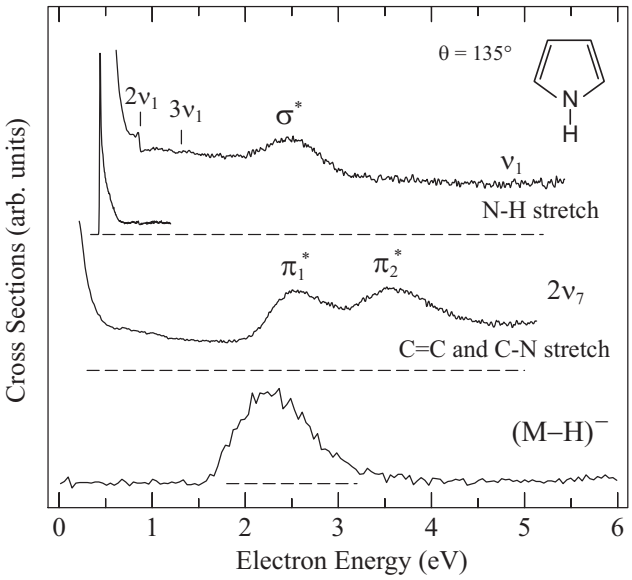

Figure 1.33: Cross sections for the excitation of the N−H stretch and ring breathing (C=C and C−N stretch) vibrations, and DEA (loss of H-atom).

and shows no structure in the present low resolution spectrum (Skalický and Allan 2004).

1.12 Summary and Conclusions

This chapter describes instrumental progress in the measurement of absolute cross sections, primarily for elastic scattering, vibrational excitation, and dissociative electron attachment. The progress permitted new insight, particularly into threshold structures which require that the instrument performs well at low energies, that it is sensitive because the threshold structures often appear only in the excitation of high vibrational levels, and that it has a resolution of around 10 meV.

Several compounds are then presented which may in some respects serve as prototypes for various phenomena. N_2 and CO are the prototypes for 'classical' shape resonances. They also serve as a validation of the experimental procedures – important is in particular the agreement of the 'grand total' cross section obtained 'the hard way', by integrating all differential cross sections and summing all partial cross sections, with the grand total cross section from the transmission experiment.

Hydrogen halides are important because they exhibit a number of phenomena which are challenging to describe theoretically – they require nonlocal resonance methods. Measurements of the cross sections provide data for testing these theories. Hydrogen halides also serve as prototypes for the threshold phenomena, because they exhibit a great variety of them with great clarity and simplicity inherent to diatomic molecules: threshold peaks, vibrational Feshbach resonances, cusps at vibrational thresholds, boomerang structures converging to the DEA threshold, outer well resonances, downward steps in DEA cross sections due to interchannel coupling, dipole and polarizability binding of

an electron, nonadiabatic effects. These concepts are applicable also to much larger molecules, in particular biomolecules, as has been shown both experimentally and theoretically (Scheer et al. 2004, Scheer et al. 2005, Abouaf and Dunet 2005, Burrow et al. 2006, Scheer et al. 2007, Gallup et al. 2009a, Fabrikant 2009, Fabrikant 2010, Gallup and Fabrikant 2011, Sommerfeld 2007).

Another prototype case is chlorobenzene, where the experiment shows that vertical attachment to a σ^* orbital does not lead to DEA, but that the π^* resonances, with their narrow autodetachment width, act as doorway states, whereby a distortion of the geometry by-passes the energetic barrier. Although threshold peaks are found in the VE cross sections and indicate that dipole-binding similar to the hydrogen halides case may occur, it does not appear to be important for DEA.

A π^* resonance is the doorway state also in acetylene, and quantitative calculations of the nuclear dynamics on *ab initio* resonant potential energy surface yielded results in good agreement with experiment, both in terms of the absolute value of the cross section and of the isotope effect. A major progress of these calculations is that they were carried out in several dimensions, and this is essential when symmetry is lowered during dissociation. The theory provided valuable insight into the time-dependent motion of the nuclear wave packet.

In systems with both a narrow π^* resonance and long range binding the mutual interplay of the two mechanisms is not *a priori* clear and an extension of the nonlocal methods into several dimensions would be desirable in this respect. In pyrrole, as an example, a sharp cusp at the energy of the N−H stretch excitation cross section indicates phenomena related to those in hydrogen halides, but DEA could also occur from the π^* resonance, enabled by geometry distortion similarly to the chlorobenzene and acetylene cases. Formic acid is another molecule with both cusps in VE cross sections and a π^* resonance with boomerang structure, where the DEA mechanism is not *a priori* clear.

The long range binding of the electron in nitromethane is stronger than in the above cases. The existence of both a dipole bound and a valence states of the anion were established based on experiments on Rydberg electron transfer and anion photoelectron spectroscopy, and the ground vibrational levels of both states are not resonances but are bound. Higher vibrational levels of both states appear as narrow resonances and as boomerang structure in the elastic and VE cross sections. Their role in DEA is not clear and high resolution DEA spectra would be interesting.

An important prototype is also CO_2, showing that many of the threshold phenomena are possible even without a permanent dipole moment.

N_2O could also be called a prototype because it explicitly shows VFRs acting as doorway states for DEA. This phenomenon can not occur in the hydrogen halides because (in absence of energy barriers) in the diatomic molecules the VFRs converge to the DEA threshold, *i.e.*, they are energetically below it. (VFRs can dissociate if they are behind a barrier and thus above the dissociation limit, such as in methyl iodide (Schramm et al. 1999).) In N_2O the VFRs are sustained by the bending motion, up to energies which are above the dissociation threshold, since the dissociation path starts in an orthogonal direction, along the N−O stretch. An interesting problem to be solved by theory is to clarify the nature of the coupling between the initial bending mode involved in the VFR and the final N−O stretch leading to dissociation.

Bibliography

Abouaf, R. (2008). Low energy electron impact in gas phase glycine, alanine and propanoic acid: Electronic, vibrational excitations and negative ions. *Chem. Phys. Lett. 451*(1-3), 25–30.

Abouaf, R., L. Andrić, R. Azria, and M. Tronc (1981). Dissociative attachment in C_2N_2 and C_2H_2. In S. Datz (Ed.), *Proc. 12th Int. Conf. on the Physics of Electronic and Atomic Collisions*, Amsterdam. North-Holland.

Abouaf, R. and H. Dunet (2005). Structures in dissociative electron attachment cross-sections in thymine, uracil and halouracils. *Eur. Phys. J. D 35*, 405–410.

Abouaf, R. and D. Teillet-Billy (1977). Fine structure in dissociative-attachment cross sections for hydrogen chloride and deuterium chloride. *J. Phys. B: At. Mol. Phys. 10*, 2261–2268.

Abouaf, R. and D. Teillet-Billy (1980). Fine structure in the dissociative attachment cross sections for HBr and HF. *Chem. Phys. Lett. 73*(1), 106–109.

Adaniya, H., B. Rudek, T. Osipov, D. J. Haxton, T. Weber, T. N. Rescigno, C. W. McCurdy, and A. Belkacem (2009). Imaging the molecular dynamics of dissociative electron attachment to water. *Phys. Rev. Lett. 103*(23), 233201.

Aflatooni, K., A. M. Scheer, and P. D. Burrow (2006). Total dissociative electron attachment cross ections for molecular constituents of DNA. *J. Chem. Phys. 125*, 054301.

Allan, M. (1982). Forward electron scattering in benzene; forbidden transitions and excitation functions. *Helv. Chim. Acta 65*, 2008–2023.

Allan, M. (1985). Experimental observation of structures in the energy dependence of vibrational excitation in H_2 by electron impact in the $^2\Sigma_u^+$ resonance region. *J. Phys. B 18*(13), L451.

Allan, M. (1992). Measurement of differential cross sections for excitation of helium by electron impact within the first 4 eV above threshold. *J. Phys. B: At. Mol. Opt. Phys. 25*, 1559.

Allan, M. (2000). Excitation of the 2^3S state of helium by electron impact from threshold to 24 eV: measurements with the magnetic angle changer. *J. Phys. B: At. Mol. Opt. Phys. 33*, L215.

Allan, M. (2001). Selectivity in the excitation of Fermi-coupled vibrations in CO_2 by impact of slow electrons. *Phys. Rev. Lett. 87*, 033201/1–033201/4.

Allan, M. (2002). Vibrational structures in electron-CO_2 scattering below the $^2\Pi_u$ shape resonance. *J. Phys. B: At. Mol. Opt. Phys. 35*, L387.

Allan, M. (2004). Threshold phenomena in electron-molecule scattering. *Phys. Scripta T110*(3), 161–165.

Allan, M. (2005). Measurement of the elastic and $v = 0 \rightarrow 1$ differential electron-N_2 cross sections over a wide angular range. *J. Phys. B: At. Mol. Opt. Phys. 38*, 3655–3672.

Allan, M. (2006). Study of resonances in formic acid by means of vibrational excitation by slow electrons. *J. Phys. B: At. Mol. Opt. Phys. 39*, 2939.

Allan, M. (2007a). Absolute angle-differential elastic and vibrational excitation cross sections for electron collisions with tetrahydrofuran. *J. Phys. B: At. Mol. Opt. Phys. 40*, 3531–3544.

Allan, M. (2007b). Electron collisions with formic acid monomer and dimer. *Phys. Rev. Lett. 98*, 123201.

Allan, M. (2010). Electron collisions with CO: Elastic and vibrational excitation cross sections. *Phys. Rev. A 81*, 042706/1–042706/9.

Allan, M. and L. Andrić (1996). σ^*-resonances in electron impact-induced vibrational excitation of *n*-propane, cyclopropane, ethylene oxide, cyclopentane, and cyclohexane. *J. Chem. Phys. 105*, 3559–3568.

Allan, M., M. Čížek, J. Horáček, and W. Domcke (2000). Electron scattering in cooled HCl: boomerang structures and outer-well resonances in elastic and vibrational excitation cross sections. *J. Phys. B: At. Mol. Opt. Phys. 33*, L209.

Allan, M. and I. I. Fabrikant (2002). Threshold peaks and structures in vibrational excitation of CH_3I by electron impact. *J. Phys. B: At. Mol. Opt. Phys. 35*, 1025–1034.

Allan, M. and T. Skalický (2003). Structures in elastic, vibrational, and dissociative electron attachment cross sections in N_2O near threshold. *J. Phys. B 36*, 3397.

Andrić, L. and R. I. Hall (1988). Resonance phenomena observed in electron scattering from acetylene. *J. Phys. B 21*, 355–366.

Asmis, K. R. and M. Allan (1997a). Excess energy partitioning between electrons departing at 0° and 180° in the ionization of helium near threshold. *J. Phys. B: At. Mol. Opt. Phys. 30*, L167–L173.

Asmis, K. R. and M. Allan (1997b). Measurement of absolute differential cross sections for the excitation of the $n = 2$ states of helium at 0° and 180°. *J. Phys. B: At. Mol. Opt. Phys. 30*(8), 1961–1974.

Azria, R. and F. Fiquet-Fayard (1972). Attachement électronique dissociatif sur C_2H_2 et C_2D_2. *J. Physique 33*, 663–667.

Azria, R., L. Roussier, P. Paineau, and M. Tronc (1974). Attachment electronique dissociatif sur HCl et DCl. *Rev. Phys. Apl. 9*, 469.

Azria, R., S. F. Wong, and G. J. Schulz (1975). Vibrational excitation in N_2O *via* the 2.3-eV shape resonance. *Phys. Rev. A 11*(4), 1309–1313.

Bachorz, R. A., M. Haranczyk, I. Dabkowska, J. Rak, and M. Gutowski (2005). Anion of the formic acid dimer as a model for intermolecular proton transfer induced by a π^* excess electron. *J. Chem. Phys. 122*, 204304.

Barsotti, S., E. Leber, M.-W. Ruf, and H. Hotop (2002). High resolution study of cluster anion formation in low-energy electron collisions with molecular clusters of CO_2, CS_2 and O_2. *Int. J. of Mass Spectrom. and Ion Proc. 220*, 313–330.

Bazin, M., S. Ptasinska, A. D. Bass, and L. Sanche (2009). Electron induced dissociation in condensed-phase nitromethane I: Desorption of ionic fragments. *Phys. Chem. Chem. Phys. 11*, 1610–1618.

Bazin, M., S. Ptasinska, A. D. Bass, L. Sanche, E. Burean, and P. Swiderek (2010). Electron induced dissociation in the condensed-phase nitromethane: II. Desorption of neutral fragments. *J. Phys. Cond. Mat. 22*(8), 084003.

Bettega, M. H. F., C. Winstead, and V. McKoy (2006). Low-energy electron scattering by N_2O. *Phys. Rev. A 74*(2), 022711.

Birtwistle, D. T. and A. Herzenberg (1971). Vibrational excitation of N_2 by resonance scattering of electrons. *J. Phys. B 4*, 53–70.

Boness, M. J. W. and G. J. Schulz (1974). Vibrational excitation in CO_2 *via* the 3.8-eV resonance. *Phys. Rev. A 9*(5), 1969–1979.

Brunger, M. J., P. J. O. Teubner, A. M. Weigold, and S. J. Buckman (1989). Vibrational excitation of nitrogen in the $^2\Pi_g$ resonance region. *J. Phys. B: At. Mol. Opt. Phys. 22*, 1443–1453.

Buckman, S. J. and B. Lohmann (1986). Electron scattering from CO in the $^2\Pi$ resonance region. *Phys. Rev. A 34*, 1561–1563.

Bulliard, C., M. Allan, and E. Haselbach (1994). Intramolecular competition of phenylic and benzylic CX bond breaking in dissociative electron attachment to dihalotoluenes. *J. Phys. Chem. 98*, 11040–5.

Burrow, P. D., G. A. Gallup, A. M. Scheer, S. Denifl, S. Ptasińska, T. Märk, and P. Scheier (2006). Vibrational feshbach resonances in uracil and thymine. *J. Chem. Phys. 124*, 124310/1–124310/7.

Campbell, L. and M. J. Brunger (2008). Electron cooling by carbon monoxide in the atmospheres of Mars and Venus. *PMC Phys. B 1:3*.

Campbell, L. and M. J. Brunger (2009a). Electron impact excitation of carbon monoxide in comet Hale-Bopp. *Geophys. Res. Lett. 36*, LO3101.

Campbell, L. and M. J. Brunger (2009b). On the role of electron-driven processes in planetary atmospheres and comets. *Physica Scripta 80*, 058101.

Chaney, E. L. and L. G. Christophorou (1969). Electron attachment to N_2O. *J. Chem. Phys. 51*, 883–893.

Chantry, P. J. (1969). Temperature dependence of dissociative attachment in N_2O. *J. Phys. Chem. 51*, 3369–3380.

Cho, H., Y. S. Park, H. Tanaka, and S. J. Buckman (2004). Measurements of elastic electron scattering by water vapour extended to backward angles. *J. Phys. B 37*, 625.

Chourou, S. T. and A. E. Orel (2008). Dissociative attachment to acetylene. *Phys. Rev. A 77*(4), 042709.

Chourou, S. T. and A. E. Orel (2009a). Dissociative electron attachment to HCCH, HCN and HCCCN. *J. Phys. Conf. Ser. 194*(5), 052032.

Chourou, S. T. and A. E. Orel (2009b). Dissociative electron attachment to HCN and HNC. *Phys. Rev. A 80*, 032709.

Chourou, S. T. and A. E. Orel (2009c). Improved calculation on the isotope effect in dissociative electron attachment to acetylene. *Phys. Rev. A 80*(3), 034701.

Čížek, M., J. Horáček, M. Allan, and W. Domcke (2002). Resonances and threshold phenomena in low-energy electron collisions with hydrogen halides: New experimental and theoretical results. *Czechosl. J. Phys. 52*, 1057–1070.

Čížek, M., J. Horáček, M. Allan, I. I. Fabrikant, and W. Domcke (2003). Vibrational excitation of hydrogen fluoride by low-energy electrons: Theory and experiment. *J. Phys. B 36*, 2837–2849.

Čížek, M., J. Horáček, M. Allan, A.-C. Sergenton, D. Popović, W. Domcke, T. Leininger, and F. X. Gadea (2001). Inelastic low-energy electron collisions with the HBr molecule: experiment and theory. *Phys. Rev. A 63*, 062710.

Compton, R. N., H. S. J. Carman, C. Desfrancois, H. Abdoul-Carmine, J. P. Schermann, J. H. Hendricks, S. A. Lyapustina, and K. H. Bowen (1996). On the binding of electrons to nitromethane: Dipole and valence bound anions. *J. Chem. Phys. 105*(9), 3472–3478.

Cvejanović, S. (1993). In T. Andersen et al. (Eds.), *The Physics of Electronic and Atomic Collisions*, pp. 390. Proceedings of the XVIII ICPEAC, Aarhus: American Institute of Physics, New York.

Cvejanovic, S. and J. Jureta (1989). In *3rd Eur. Conf. on Atomic and Molecular Physics (Bordeaux)*, unpublished, pp. 638.

Deak, J. C., L. K. Iwaki, and D. D. Dlott (1999). Vibrational energy redistribution in polyatomic liquids: Ultrafast IR-raman spectroscopy of nitromethane. *J. Phys. Chem. A 103*(8), 971–979.

Denifl, S., V. Vizcaino, T. D. Märk, E. Illenberger, and P. Scheier (2010). High resolution electron attachment to CO_2 clusters. *Phys. Chem. Chem. Phys. 12*, 5219–5224.

Dessent, C. E. H., J. Kim, and M. A. Johnson (2000). Spectroscopic observation of vibrational Feshbach resonances in near-threshold photoexcitation of $X^- \cdot CH_3NO_2$ ($X^- = I^-$ and Br^-). *Faraday Discuss. 115*, 395–406.

Domcke, W. (1989). In A. Herzenberg (Ed.), *Aspects of Electron-Molecule Scattering and Photoionization*, Number 204 in AIP Conference Proceedings, pp. 169–180. American Institute of Physics.

Domcke, W. (1991). Theory of resonance and threshold effects in electron-molecule collisions: The projection-operator approach. *Phys. Rep. 208*, 97.

Dorman, F. H. (1966). Negative fragment ions from resonance capture processes. *J. Chem. Phys. 44*, 3856–3863.

Dressler, R. and M. Allan (1987). A dissociative electron attachment, electron transmission, and electron energy-loss study of the temporary negative ion of acetylene. *J. Chem. Phys. 87*, 4510–4518.

Dubé, L. and A. Herzenberg (1975). Resonant electron-molecule scattering: The impulse approximation in N_2O. *Phys. Rev. A 11*(4), 1314–1325.

Dubé, L. and A. Herzenberg (1979). Absolute cross sections from the "boomerang model" for resonant electron-molecule scattering. *Phys. Rev. A 20*(1), 194–213.

Estrada, H., L. S. Cederbaum, and W. Domcke (1986). Vibronic coupling of short-lived electronic states. *J. Chem. Phys. 84*, 152.

Estrada, H. and W. Domcke (1985). On the virtual state effect in low-energy electron-CO_2 scattering. *J. Phys. B: At. Mol. Phys. 18*, 4469–4479.

Fabrikant, I. I. (1990). Resonance processes in e-HCl collisions; comparison of the R-matrix and the nonlocal-complex potential methods. *Comm. At. Mol. Phys. 24*, 37.

Fabrikant, I. I. (2009). Dissociative electron attachment: Threshold phenomena and multimode effects. *J. Phys. Conf. Ser. 192*(1), 012002.

Fabrikant, I. I. (2010). Recent progress in the theory of dissociative attachment: from diatomics to biomolecules. *J. Phys. Conf. Ser. 204*, 012004.

Fedor, J., O. May, and M. Allan (2008). Absolute cross sections for dissociative electron attachment to HCl, HBr and their deuterated analogues. *Phys. Rev. A 78*, 032701.

Fedor, J., C. Winstead, V. McKoy, M. Čížek, K. Houfek, P. Kolorenč, and J. Horáček (2010). Electron scattering in HCl: an improved nonlocal resonance model. *Phys. Rev. A 81*, 042702.

Feng, H., W. Sun, and M. A. Morrison (2003). Importance of nonresonant scattering in low-energy dissociative electron attachment to molecular hydrogen. *Phys. Rev. A 68*, 062709.

Feng, H., W. Sun, and M. A. Morrison (2005). *private communication*.

Gallup, G. A., P. D. Burrow, and I. I. Fabrikant (2009a). Electron-induced bond breaking at low energies in HCOOH and glycine: The role of very short-lived σ^* anion states. *Phys. Rev. A 79*(4), 042701.

Gallup, G. A., P. D. Burrow, and I. I. Fabrikant (2009b). Reply to Comment on electron-induced bond breaking at low energies in HCOOH and glycine: The role of very short-lived σ^* anion states. *Phys. Rev. A 80*(4), 046702.

Gallup, G. A. and I. I. Fabrikant (2007). Resonances and threshold effects in low-energy electron collisions with methyl halides. *Phys. Rev. A 75*(3), 032719.

Gallup, G. A. and I. I. Fabrikant (2011). Vibrational feshbach resonances in dissociative electron attachment to uracil. *Phys. Rev. A 83*(1), 012706.

Gauyacq, J. P. (1987). *Dynamics of Negative Ions*. World Scientific.

Gianturco, F. A. and R. R. Lucchese (2004). Nanoscopic models for radiobiological damage: metastable precursors of dissociative electron attachment to formic acid. *New J. Phys. 6*, 66.

Gianturco, F. A., R. R. Lucchese, J. Langer, I. Martin, M. Stano, G. Karwasz, and E. Illenberger (2005). Modelling electron-induced processes in condensed formic acid: Resonant states of $(HCOOH)_2$ at low energies. *Eur. Phys. J. D 35*, 417.

Gibson, J. C., L. A. Morgan, R. J. Gulley, M. J. Brunger, C. T. Bundschu, and S. J. Buckman (1996). Low energy electron scattering from CO: Absolute cross section measurements and R-matrix calculations. *J. Phys. B: At. Mol. Opt. Phys. 29*, 3197–3214.

Gilbert, S. J., C. Kurz, R. G. Greaves, and C. M. Surko (1997). Creation of a monoenergetic pulsed positron beam. *Appl. Phys. Lett. 70*, 1944–1946.

Gopalan, A., J. Bömmels, S. Götte, A. Landwehr, K. Franz, M. W. Ruf, H. Hotop, and K. Bartschat (2003). A novel electron scattering apparatus combining a laser photoelectron source and a triply differentially pumped supersonic beam target: characterization and results for the $He^-(1s2s^2)$ resonance. *Eur. Phys. J. D 22*, 17.

Gribakin, G. F., J. A. Young, and C. M. Surko (2010). Positron-molecule interactions: Resonant attachment, annihilation, and bound states. *Rev. Mod. Phys. 82*(3), 2557–2607.

Gutsev, G. L. and R. J. Bartlett (1996). A theoretical study of the valence- and dipole-bound states of the nitromethane anion. *J. Chem. Phys. 105*(19), 8785–8792.

Hake, Jr., R. D. and A. V. Phelps (1967). Momentum-transfer and inelastic-collision cross sections for electrons in O_2, CO, and CO_2. *Phys. Rev. 158*, 70–84.

Horáček, J., W. Domcke, and H. Nakamura (1997). Electron attachment and vibrational excitation in hydrogen iodide: Calculations based on the nonlocal resonance model. *Z. Phys. D 42*, 181–185.

Horáček, J. (2000). Inelastic low-energy electron collisions with hydrogen halides. In Y. Itikawa et al. (Eds.), *The Physics of Electronic and Atomic Collisions*, Volume 500, pp. 329. Proceedings of the XXIICPEAC, Sendai 1999: American Institute of Physics, New York.

Hotop, H., M.-W. Ruf, M. Allan, and I. I. Fabrikant (2003). Resonance and threshold phenomena in low-energy electron collisions with molecules and clusters. *Adv. At. Mol. Opt. Phys. 49*, 85.

Ibanescu, B. C. and M. Allan (2009). Selectivity in bond cleavage in amines and thiols by dissociative electron attachment. *J. Phys.: Conf. Ser. 194*, 012030.

Ibănescu, B. C., O. May, A. Monney, and M. Allan (2007). Electron-induced chemistry of alcohols. *Phys. Chem. Chem. Phys. 9*, 3163–3173.

Itikawa, Y. (2002). Cross sections for electron collisions with carbon dioxide. *J. Phys. Chem. Ref. Data 31*, 749–767.

Jung, K., T. Antoni, R. Müller, K.-H. Kochem, and H. Ehrhardt (1982). Rotational excitation of N_2, CO and H_2O by low-energy electron collisions. *J. Phys. B: At. Mol. Phys. 15*, 3535–3555.

Kanik, I., S. Trajmar, and J. C. Nickel (1993). Total electron scattering and electronic state excitations cross sections for O_2, CO, and CH_4. *J. Geophys. Res. 98*, 7447.

Knoth, G., M. Gote, M. Rädle, K. Jung, and H. Ehrhardt (1989). Nuclear-excited Feshbach resonances in the electron scattering from hydrogen halides. *Phys. Rev. Lett. 62*(15), 1735–1737.

Knudsen, M. (1910). Eine Revision der Gleichgewichtsbedingung der Gase. Thermische Molekularströmung. *Ann. Phys. 31*, 205–229.

Ko, Y. J., H. Wang, D. Radisic, S. T. Stokes, S. N. Eustis, K. H. Bowen, K. Mazurkiewicz, P. Storoniak, A. Kowalczyk, M. Haranczyk, M. Gutowski, and J. Rak (2010). Barrier-free proton transfer induced by electron attachment to the complexes between 1-methylcytosine and formic acid. *Mol. Phys. 108*, 2621–2631.

Krishnakumar, E. and S. K. Srivastava (1990). Dissociative attachment of electrons to N_2O. *Phys. Rev. A 41*(5), 2445–2452.

Kwan, C. K., Y. F. Hsieh, W. E. Kauppila, S. J. Smith, T. S. Stein, M. N. Uddin, and M. S. Dababneh (1983). $e^{\pm}$-CO and $e^{\pm}$-CO_2 total cross-section measurements. *Phys. Rev. A 27*(3), 1328–1336.

Lecomte, F., S. Carles, C. Desfrancois, and M. A. Johnson (2000). Dipole bound and valence state coupling in argon-solvated nitromethane anions. *J. Chem. Phys. 113*(24), 10973.

Lunt, S. L., D. Field, J.-P. Ziesel, N. C. Jones, and R. J. Gulley (2001). Very low energy electron scattering in nitromethane, nitroethane, and nitrobenzene. *Int. J. Mass Spectr. 205*(1-3), 197–208.

Martin, I., T. Skalický, J. Langer, H. Abdoul-Carime, G. Karwasz, E. Illenberger, M. Stano, and S. Matejcik (2005). Low energy electron driven reactions in single formic acid molecules (HCOOH) and their homogeneous clusters. *Phys. Chem. Chem. Phys. 7*, 2212.

May, O., J. Fedor, and M. Allan (2009). Isotope effect in dissociative electron attachment to acetylene. *Phys. Rev. A 80*, 012706.

May, O., J. Fedor, B. C. Ibănescu, and M. Allan (2008). Absolute cross sections for dissociative electron attachment to acetylene and diacetylene. *Phys. Rev. A 77*, 040701(R).

May, O., D. Kubala, and M. Allan (2010). Absolute cross sections for dissociative electron attachment to HCN and DCN. *Phys. Rev. A 82*(1), 010701.

Michaud, M., E. M. Hébert, P. Cloutier, and L. Sanche (1997). Charge trapping and the desorption of anionic and metastable fragments by dissociative electron attachment to condensed N_2O. *J. Phys. B: At. Mol. Opt. Phys. 30*, 3527–3541.

Michaud, M., E. M. Hébert, P. Cloutier, and L. Sanche (2007). Electron photoemission from charged films: Absolute cross section for trapping 0–5 eV electrons in condensed CO_2. *J. Chem. Phys. 126*(2), 024701.

Modelli, A. (2005). Empty level structure and dissociative electron attachment cross section in (bromoalkyl)benzenes. *J. Phys. Chem. A 109*(28), 6193–6199.

Moore, J. H., P. Swiderek, S. Matejcik, and M. Allan (2010). Fundamentals of interactions of electrons with molecules. In P. Russell, I. Utke, and S. Moshkalev (Eds.),

Nanofabrication Using Focused Ion and Electron Beams: Principles and Applications, pp. in press. Oxford University Press.

Morgan, L. A. (1991). Low-energy electron scattering by CO. *J. Phys. B: At. Mol. Opt. Phys. 24*(21), 4649–4660.

Morgan, L. A. (1998). Virtual states and resonances in electron scattering by CO_2. *Phys. Rev. Lett. 80*, 1873–1875.

Motlagh, S. and J. H. Moore (1998). Cross sections for radicals from electron impact on methane and fluoroalkanes. *J. Chem. Phys. 109*, 432.

Mündel, C., M. Berman, and W. Domcke (1985). Nuclear dynamics in resonant electron-molecule scattering beyond the local approximation: Vibrational excitation and dissociative attachment in H_2 and D_2. *Phys. Rev. A 32*(1), 181–193.

Murphy, T. J. and C. M. Surko (1992). Positron trapping in an electrostatic well by inelastic collisions with nitrogen molecules. *Phys. Rev. A 46*, 5696–5705.

Nandi, D., V. S. Prabhudesai, B. M. Nestmann, and E. Krishnakumar (2011). Dissociative electron attachment to NO probed by velocity map imaging. *Phys. Chem. Chem. Phys. 13*, 1542–1551.

Nesbet, R. K. (1979). Variational calculations of accurate e^-−He cross sections below 19 eV. *Phys. Rev. A 20*, 58–70.

Nickel, J. C., P. W. Zetner, G. Shen, and S. Trajmar (1989). Principles and procedures for determining absolute differential electron-molecule (atom) scattering cross sections. *J. Phys. E: Sci. Instrum. 22*, 730.

Orient, O. J. and S. K. Srivastava (1983). Production of O^- from CO_2 by dissociative electron attachment. *Chem. Phys. Lett. 96*, 681–684.

Pavlovic, Z., M. J. W. Boness, A. Herzenberg, and G. J. Schulz (1972). Vibrational excitation in molecular nitrogen by electron impact in the 15-35 eV region. *Phys. Rev. A 6*, 676–685.

Pelc, A., W. Sailer, P. Scheier, and T. D. Märk (2005). Generation of $(M\text{-}H)^-$ ions by dissociative electron attachment to simple organic acids M. *Vacuum 78*, 631–634.

Pelc, A., W. Sailer, P. Scheier, N. Mason, and T. Märk (2002). Low energy electron attachment to formic acid. *Eur. Phys. J. D 20*, 441–444.

Pelc, A., W. Sailer, P. Scheier, N. J. Mason, E. Illenberger, and T. D. Märk (2003). Electron attachment to simple organic acids. *Vacuum 70*, 429.

Pelc, A., W. Sailer, P. Scheier, M. Probst, N. J. Mason, E. Illenberger, and T. D. Märk (2002). Dissociative electron attachment to formic acid (HCOOH). *Chem. Phys. Lett. 361*(3-4), 277–284.

Pichou, F., A. Huetz, G. Joyez, and M. Landau (1978). Near threshold ionization of helium by electron impact. *J. Phys. B 11*, 3683–3692.

Poparić, G. B., D. S. Belić, and M. D. Vićić (2006). Resonant vibrational excitation of CO by low-energy electrons. *Phys. Rev. A 73*, 062713/1–062713/6.

Poparić, G. B., S. M. D. Galijaš, and D. S. Belić (2004). Forward-to-backward differential-cross-section ratio in electron-impact vibrational excitation *via* the $^2\Pi$ resonance of CO. *Phys. Rev. A 70*(2), 024701.

Poparić, G. B., D. S. Belić, and M. M. Ristić (2010). Resonant vibrational excitation of H_2 by electron impact: Full-range differential cross sections. *Phys. Rev. A 82*(1), 012706/1–012706/5.

Prabhudesaia, V. S., D. Nandia, A. H. Kelkara, R. Parajulib, and E. Krishnakumar (2005). Dissociative electron attachment to formic acid. *Chem. Phys. Lett. 405*, 172–176.

Ptasinska, S., S. Denifl, P. Scheier, E. Illenberger, and T. D. Märk (2005). Bond- and site-selective loss of H atoms from nucleobases by very-low-energy electrons (<3 eV). *Angew. Chem. Int. Ed. 44*, 6941–6943.

Ramsauer, C. and R. Kollath (1929). Über den Wirkungsquerschnitt der Edelgasmoleküle gegenüber Elektronen unterhalb 1 Volt. *Ann. Physik (Leipzig) 3*, 536.

Ramsauer, C. and R. Kollath (1930). Über den Wirkungsquerschnitt der Nichtedelgasmoleküle gegenüber Elektronen unterhalb 1 Volt. *Ann. Physik (Leipzig) 4*, 91.

Rapp, D. and D. D. Briglia (1965). Total cross sections for ionization and attachment in gases by electron impact. II. Negative-ion formation. *J. Chem. Phys. 43*, 1480–1490.

Read, F. H. (1975). Doppler and other broadening effects in electron scattering experiments. *J. Phys. B 8*, 1034–1040.

Read, F. H. and N. J. Bowring (2005). The CPO-3D program. www.electronoptics.com.

Read, F. H. and J. M. Channing (1996). Production and optical properties of an unscreened but localized magnetic field. *Rev. Sci. Instrum. 67*, 2373.

Rescigno, T. N., C. W. McCurdy, D. J. Haxton, C. S. Trevisan, and A. E. Orel (2007). Nuclear dynamics in resonant electron collisions with small polyatomic molecules. *J. Phys. Conf. Ser. 88*, 012027–012035.

Rescigno, T. N., C. S. Trevisan, and A. E. Orel (2006). Dynamics of low-energy electron attachment to formic acid. *Phys. Rev. Lett. 96*, 213201.

Rescigno, T. N., C. S. Trevisan, and A. E. Orel (2009). Comment on electron-induced bond breaking at low energies in HCOOH and glycine: The role of very short-lived σ^* anion states. *Phys. Rev. A 80*(4), 046701.

Rohr, K. (1978). Interaction mechanisms and cross sections for the scattering of low-energy electrons from HBr. *J. Phys. B 11*(10), 1849.

Rohr, K. and F. Linder (1975). Vibrational excitation in e-HCl collisions at low energies. *J. Phys. B: At. Mol. Phys. 8*, L200.

Sailer, W., A. Pelc, S. Matejcik, E. Illenberger, P. Scheier, and T. D. Märk (2002). Dissociative electron attachment study to nitromethane. *J. Chem. Phys. 117*, 7989–7994.

Schafer, O. and M. Allan (1991). Measurement of near-threshold vibrational excitation of HCl by electron impact. *Journal of Physics B: Atomic, Molecular and Optical Physics 24*(13), 3069.

Scheer, A. M., K. Aflatooni, G. A. Gallup, and P. D. Burrow (2004). Bond breaking and temporary anion states in uracil and halouracils: Implications for the DNA bases. *Phys. Rev. Lett. 92*, 068102.

Scheer, A. M., P. Możejko, G. A. Gallup, and P. D. Burrow (2007). Total dissociative electron attachment cross sections of selected amino acids. *J. Chem. Phys. 126*, 174301.

Scheer, A. M., C. Silvernail, J. A. Belot, K. Aflatooni, G. A. Gallup, and P. D. Burrow (2005). Dissociative electron attachment to uracil deuterated at the N_1 and N_3 positions. *Chemical Physics Letters 411*(1-3), 46–50.

Schramm, A., I. I. Fabrikant, J. M. Weber, E. Leber, M.-W. Ruf, and H. Hotop (1999). Vibrational resonance and threshold effects in inelastic electron collisions with methyl iodide molecules. *J. Phys. B: At. Mol. Opt. Phys. 32*, 2153–2171.

Schulz, G. J. (1973). Resonances in electron impact on diatomic molecules. *Rev. Mod. Phys. 45*, 423.

Sergenton, A.-C. and M. Allan (2000). Excitation of vibrational levels of HI up to $v = 8$ by electron impact. *Chem. Phys. Lett. 319*(1-2), 179 – 183.

Sergenton, A.-C., L. Jungo, and M. Allan (2000). Excitation of vibrational levels of HF up to $v = 4$ by electron impact. *Phys. Rev. A 61*(6), 062702.

Shi, X., T. M. Stephen, and P. D. Burrow (1993). Differential cross sections for elastic scattering of electrons from molecular nitrogen at 0.55, 1.5, and 2.2 eV. *J. Phys. B: At. Mol. Opt. Phys. 26*, 121–128.

Skalický, T. and M. Allan (2004). The assignment of dissociative electron attachment bands in compounds containing hydroxyl and amino groups. *J. Phys. B 37*, 4849.

Skalický, T., C. Chollet, N. Pasquier, and M. Allan (2002). Properties of the π^* and σ^* states of clorobenzene anion determined by electron impact spectroscopy. *Phys. Chem. Chem. Phys. 4*, 3583.

Sohn, W., K.-H. Kochem, K. Jung, H. Ehrhardt, and E. S. Chang (1985). Electron scattering from CO below resonance energy. *J. Phys. B: At. Mol. Phys. 18*, 2049–2055.

Sommerfeld, T. (2002). Coupling between dipole-bound and valence states: the nitromethane anion. *Phys. Chem. Chem. Phys. 4*, 2511–2516.

Sommerfeld, T. (2003). A fresh look at the $^2A_1$ CO_2^- potential energy surface. *J. Phys. B: At. Mol. Opt. Phys. 36*, L127–L133.

Sommerfeld, T. (2007). Doorway mechanism for dissociative electron attachment to fructose. *J. Chem. Phys. 126*, 124301.

Sommerfeld, T. (2008). Dipole-bound states as doorways in (dissociative) electron attachment. *J. Chem. Phys. 4*, 245.

Sommerfeld, T., H.-D. Meyer, and L. S. Cederbaum (2003). Potential energy surface of the CO_2^- anion. *Phys. Chem. Chem. Phys. 6*, 42–45.

Stamatovic, A. and G. J. Schulz (1968). Trochoidal electron monochromator. *Rev. Sci. Instrum. 39*, 1752.

Stricklett, K. L., S. C. Chu, and P. D. Burrow (1986). Dissociative attachment in vinyl and allyl chloride, chlorobenzene and benzyl chloride. *Chem. Phys. Lett. 131*, 279–284.

Sullivan, J. P., A. Jones, P. Caradonna, C. Makochekanwa, and S. J. Buckman (2008). A positron trap and beam apparatus for atomic and molecular scattering experiments. *Rev. Sci. Instrum. 79*, 113105/1–113105/5.

Sun, W., M. A. Morrison, W. A. Isaacs, A. D. T. Trail, W K, R. J. Gulley, M. J. Brennan, and S. J. Buckman (1995). Detailed theoretical and experimental analysis of low-energy electron-N_2 scattering. *Phys. Rev. A 52*, 1229.

Sweeney, C. J. and T. W. Shyn (1997). Measurement of absolute differential cross sections for the vibrational excitation of molecular nitrogen by electron impact in the $^2\Pi_g$ shape resonance region. *Phys. Rev. A 56*, 1348.

Szmytkowski, C., K. Maciag, and G. Karwasz (1996). Absolute electron-scattering total cross section measurements for noble gas atoms and diatomic molecules. *Phys. Scripta 54*(3), 271–280.

Tanaka, H., H. Toyda, and H. Sugai (1998). Cross sections for electron-impact dissociation of alternative etching gas, C_3HF_7O. *Jpn. J. Appl. Phys. 37*, 5053.

Teillet-Billy, D. and J. P. Gauyacq (1984). Dissociative attachment in e^--HCl, DCl collisions. *J. Phys. B: At. Mol. Phys. 17*, 4041–4058.

Vanroose, W., Z. Zhang, C. W. McCurdy, and T. N. Rescigno (2004). Threshold vibrational excitation of CO_2 by slow electrons. *Phys. Rev. Lett. 92*, 053201.

Vizcaino, V., S. Denifl, T. D. Märk, E. Illenberger, and P. Scheier (2010). Low energy (0-4 eV) electron impact to N_2O clusters: Dissociative electron attachment, ion-molecule reactions, and vibrational Feshbach resonances. *J. Chem. Phys. 133*, 154512/1–6.

Walker, I. C., A. Stamatovic, and S. F. Wong (1978). Vibrational excitation of ethylene by electron impact: 1-11 eV. *J. Chem. Phys. 69*, 5532.

Weber, J. M., E. Leber, M.-W. Ruf, and H. Hotop (1999). Nuclear-excited Feshbach resonances in electron attachment to molecular clusters. *Phys. Rev. Lett. 82*(3), 516–519.

Wilde, R. S., G. A. Gallup, and I. I. Fabrikant (2000). Comparative studies of dissociative electron attachment to methyl halides. *J. Phys. B: At. Mol. Opt. Phys. 33*, 5479–5492.

Zubek, M., N. Gulley, G. C. King, and F. H. Read (1996). Measurements of elastic electron scattering in the backward hemisphere. *J. Phys. B: At. Mol. Opt. Phys. 29*, L239.

Zubek, M., B. Mielewska, and G. C. King (2000). Absolute differential cross sections for electron elastic scattering and vibrational excitation in nitrogen in the angular range from 120° to 180°. *J. Phys. B: At. Mol. Opt. Phys. 33*, L527.